$Na_V1.1$ is essential for proprioceptive signaling and motor behaviors

Cyrrus M. Espino[1], Cheyanne M. Lewis[1], Serena Ortiz[2], Miloni S. Dalal[3], Snigdha Garlapalli[4], Kaylee M. Wells[5], Darik A. O'Neil[5], Katherine A. Wilkinson[2], and Theanne N. Griffith[1,5]*

[1]*Department of Physiology and Membrane Biology, University of California Davis, Davis, CA, 95616*
[2]*Department of Biological Science, San José State University, San José, CA, 95192*
[3]*Department of Pharmacology, Physiology, and Neuroscience, New Jersey Medical School-Rutgers University, Newark, NJ, 07103*
[4]*Undergraduate program in Psychology, University of California Davis, Davis, CA, 95616*
[5]*Neurobiology course, Marine Biological Laboratory Woods Hole, MA, 02540*

*Corresponding Author: Theanne N. Griffith
1275 Med Science Drive
Tupper Hall 4135
Davis, CA 95616
530.754.2780
tgriffith@ucdavis.edu

Conflicts of Interest: None to declare

Acknowledgements: This research was supported by a Postdoctoral Enrichment Program Award from the Burroughs Welcome Fund (TNG) and by 5T32GM099608-10 and 1T32GM1144303-01A1 (CME). Work at San José State was supported by NIGMS 5SC3GM127195 (KAW) and NIGMS 5R25GM71381 (SO). Core facilities were supported by P30 EY12576. Part of this project was carried out at the Marine Biological Laboratory Neurobiology Course, with support from NINDS R25NS063307. Thanks to Drs. Jon Sack and Xinzhong Dong for sharing mouse lines, Drs. Jorge Contreras and Ioana Carcea for sharing behavioral equipment, Miguel Gonzalez Fernandez for writing code to automate *ex vivo* data analysis, and members of the Griffith laboratory for helpful discussions.

ABSTRACT

The voltage-gated sodium channel (Na_V), $Na_V1.1$, is well-studied in the central nervous system; conversely, its contribution to peripheral sensory neuron function is more enigmatic. Here, we identify a new role for $Na_V1.1$ in mammalian proprioception. RNAscope analysis and *in vitro* patch clamp recordings in genetically identified mouse proprioceptors show ubiquitously channel expression and significant contributions to intrinsic excitability. Notably, genetic deletion of $Na_V1.1$ in sensory neurons caused profound and visible motor coordination deficits in conditional knockout mice of both sexes, similar to conditional Piezo2-knockout animals, suggesting this channel is a major contributor to sensory proprioceptive transmission. *Ex vivo* muscle afferent recordings conditional knockout mice found that loss of $Na_V1.1$ leads to inconsistent and unreliable proprioceptor firing characterized by action potential failures during static muscle stretch; conversely, afferent responses to dynamic vibrations were unaffected. This suggests that while a combination of Piezo2 and other Na_V isoforms are sufficient to elicit activity in response to transient stimuli, $Na_V1.1$ is required for transmission of receptor potentials generated during sustained muscle stretch. Impressively, recordings from afferents of heterozygous conditional knockout animals were similarly impaired, and heterozygous conditional knockout mice also exhibited motor behavioral deficits. Thus, $Na_V1.1$ haploinsufficiency in sensory neurons impairs both proprioceptor function and motor behaviors. Importantly, human patients harboring $Na_V1.1$ loss-of-function mutations often present with motor delays and ataxia; therefore, our data suggest sensory neuron dysfunction contributes to the clinical manifestations of neurological disorders in which $Na_V1.1$ function is compromised. Collectively, we present the first evidence that $Na_V1.1$ is essential for mammalian proprioceptive signaling and behaviors.

INTRODUCTION

Voltage gated sodium channels (Na_Vs) are critical mediators of neuronal excitability and are responsible for action potential generation and propagation (Ahern et al., 2016; Bean, 2007) . In the mammalian nervous system there are nine isoforms (Na_V1.1-1.9), each with unique biophysical properties, as well as distinguishing cellular expression and subcellular localization patterns (Bennett et al., 2019; Catterall, 2017). Of these different subtypes, Na_V1.1 is notable for its role in brain disease (Escayg and Goldin, 2010; Mulley et al., 2005; Ogiwara et al., 2007). Indeed, *Scn1a*, the gene that encodes Na_V1.1, is referred to as a "super culprit" gene, with over 1,000 associated mutations that lead to abnormal brain function, resulting in brain disorders such as epilepsy and migraine, as well as neurodivergent phenotypes, such as autism spectrum disorder (Ding et al., 2021; Lossin, 2009). Homozygous *Scn1a*$^{-/-}$ global knockout mice are ataxic and die by P15, while heterozygous *Scn1a*$^{+/-}$ animals develop seizures and begin to die sporadically starting at P21 (Yu et al., 2006). In addition to the central nervous system, Na_V1.1 is also expressed in the peripheral nervous system (Sharma et al., 2020; Usoskin et al., 2015); yet, the prominent role this channel plays in brain function has left its physiological roles in sensory neuron populations understudied.

Peripheral sensory neurons of the dorsal root and trigeminal ganglia (DRG and TG, respectively) are tasked with encoding somatic sensations, such as touch, temperature, pain, and proprioception, and are anatomically and functionally heterogenous (Kupari et al., 2021; Nguyen et al., 2021; Oliver et al., 2021a; Wu et al., 2021). *Scn1a* transcript and protein have been observed primarily in myelinated mechanosensory DRG and TG neurons (Fukuoka et al., 2008; Ho and O'Leary, 2011; Osteen et al., 2016). Indeed, subcutaneous injection of the Na_V1.1 activator, Hma1, into mouse hind paw causes non-inflammatory mechanical pain and spontaneous pain behaviors (Osteen et al., 2016). Interestingly, pharmacological inhibition of Na_V1.1 does not affect mechanical thresholds in uninjured mice but does reduce mechanical pain

in a spared-nerve injury model (Salvatierra et al., 2018), suggesting $Na_V1.1$ may have a more prominent role in mechanical pain as opposed to normal touch sensing. $Na_V1.1$ in TG neurons has also been reported to mediate mechanical pain in an orbitofacial chronic constriction injury model (Pineda-Farias et al., 2021). In addition to somatosensory neurons, $Na_V1.1$ is found in colon-innervating vagal neurons, where it contributes to firing of colonic mechano-nociceptors and is upregulated in a mouse model of chronic visceral hypersensitivity (Osteen et al., 2016; Salvatierra et al., 2018). Lastly, $Na_V1.1$ contributes to action potential firing in a subset of DRG neurons that express the cold sensitive ion channel, transient receptor potential melastatin 8 (TRPM8), suggesting the channel may also contribute to thermosensory transmission (Griffith et al., 2019). While most data support a role for $Na_V1.1$ in pain, the limited number of studies that have investigated $Na_V1.1$ function in sensory neurons has left gaps in our knowledge regarding other potential roles this channel may play in somatosensation.

Given the relatively under-explored role of $Na_V1.1$ in the peripheral nervous system, we set out to determine what other somatosensory modalities rely on $Na_V1.1$ expression in sensory neurons. Here, we show that 100% of proprioceptors express *Scn1a* mRNA, where it makes notable contributions to the somal whole-cell sodium current and intrinsic excitability. A functional role for $Na_V1.1$ in proprioceptive signaling was also supported by *ex-vivo* electrophysiological recordings from functionally identified muscle spindle afferents. Importantly, mice lacking $Na_V1.1$ in all sensory neurons display visible and profound motor deficits and ataxic-like behavior, which were quantified in rotarod and open field assays. Surprisingly, we found $Na_V1.1$ is haploinsuffcient for normal proprioceptor function and behavior, in *ex vivo* recordings and the open field assay, respectively. Collectively, our data provide the first evidence that peripherally expressed $Na_V1.1$ is critical for sensory proprioceptive signaling and motor coordination.

RESULTS

Most studies have localized $Na_V1.1$ expression primarily to myelinated sensory neurons that transmit mechanical signals (Fukuoka et al., 2008; Ho and O'Leary, 2011; Osteen et al., 2016b; Wang et al., 2011). In line with prior work, RNAscope analysis of DRG sections from adult mice showed that 93% of myelinated neurons, as determined by neurofilament heavy chain (NFH) labeling, express *Scn1a* transcripts (**Fig 1A**). RNA-sequencing datasets have consistently identified $Na_V1.1$ expression in proprioceptors; thus, we next analyzed $Na_V1.1$ expression in these cells using a $Parvalbumin^{Cre}$;$Rosa26^{Ai14}$ reporter line (*Pvalb*^{Ai14}) and found 100% of genetically identified proprioceptors were positive for *Scn1a* message (**Fig 1B**). This contrasted with low expression of *Scn1a* mRNA in both calcitonin gene related peptide (CGRP) expressing neurons, which represent peptidergic nociceptors, and non-peptidergic polymodal *Mrgprd*-expressing nociceptors (24% and 3%, respectively, **Fig 1C-D**). Frequency and cumulative distribution plots show the spread of integrated fluorescence density measurements obtained for *Scn1a* transcripts in proprioceptors (**Fig 1E-F**).

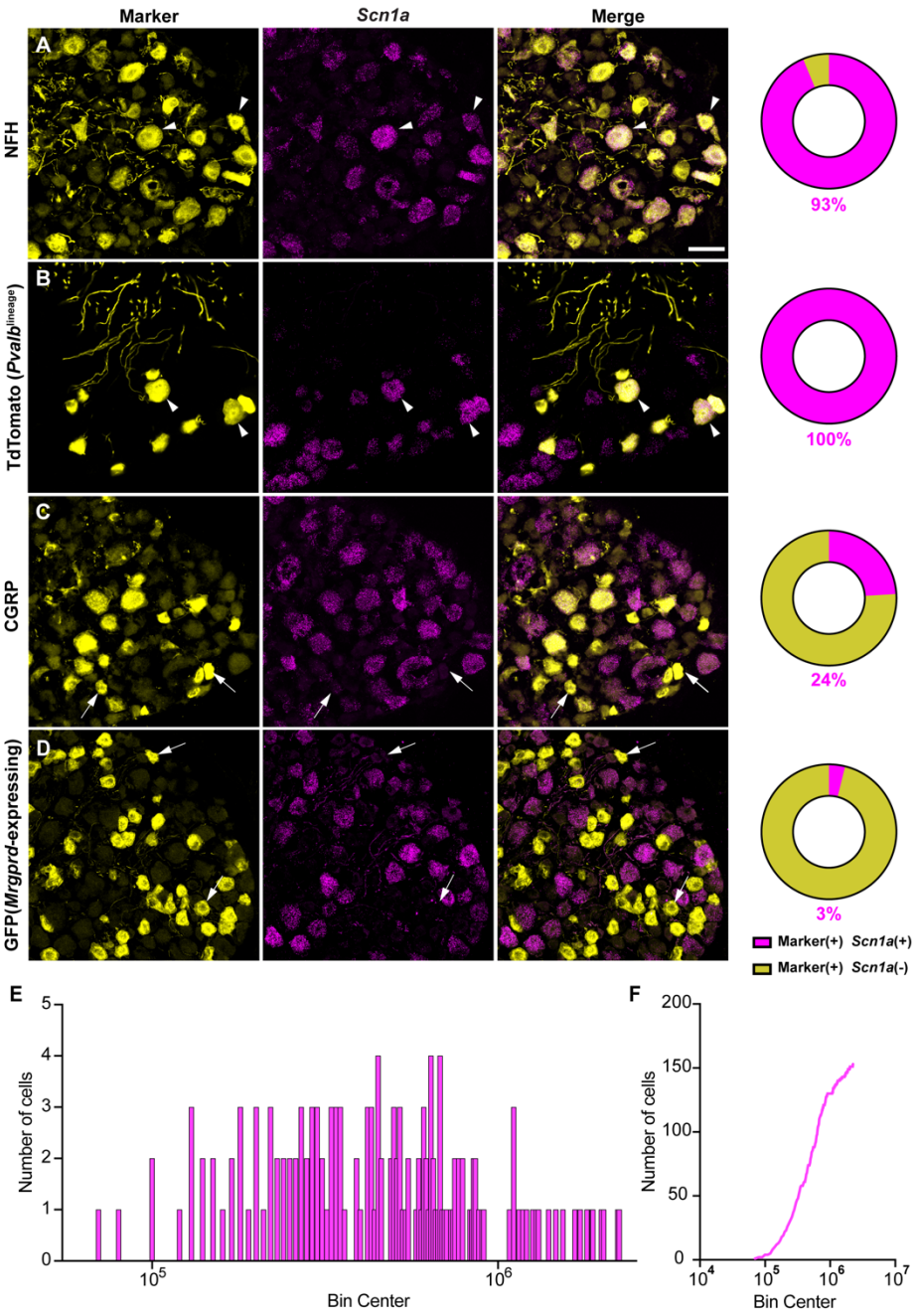

Figure 1. $Na_V1.1$ is ubiquitously expressed in genetically identified proprioceptors. **A-D**, Representative confocal images of cryoprotected adult DRG sections (25 μm) with pie chart quantifications indicating the percentage of *Scn1a*+ and *Scn1a* - neurons in each subpopulation (magenta and yellow, respectively). Images were acquired with a 40X, 0.9 NA water-immersion objective. Sections were hybridized using RNAscope with probes targeting *Scn1a* (*Scn1a*, magenta) and stained with the following antibodies (yellow): (**A**) anti-neurofilament heavy (NFH, n=787) (**B**) anti-DsRed to label TdTomato+ proprioceptors (n=143) (**C**) anti-calcitonin gene-related peptide (CGRP, n=877) and (**D**) anti-GFP to label *Mrgprd*+ neurons. DRG from C57BL/6, *Pvalb*$^{Cre;}$*Rosa26*^{Ai14}, and *Mrgprd*^{GFP} mice of both sexes were used. Scale bar 50μm. White arrowheads indicate *Scn1a* + neurons while white arrows indicate *Scn1a* - neurons. Frequency

(**E**) and cumulative (**F**) distribution plots of integrated fluorescence density of the *Scn1a* signal in TdTomato+ proprioceptors (n=153). n = cells.

In addition to $Na_V1.1$, $Na_V1.6$ and $Na_V1.7$ expression has also been reported in proprioceptors (Carrasco et al., 2017). As with *Scn1a*, mRNA for *Scn8a* and *Scn9a* is also found in 100% of genetically identified proprioceptors (**Fig 2A-B**). Cumulative distribution plots of *Scn8a* and *Scn9a* integrated fluorescence density measurements showed higher variability as compared to $Na_V1.1$ (**Fig 2C-D**, **Fig 1E**). This was quantified using the coefficient of variation, a relative measure of the extent of variations within data. The coefficient of variation for *Scn1a* transcript expression was calculated to be 75.6, whereas this value increased to 97.3 and 88.1 for *Scn8a* and *Scn9a*, respectively. This indicates that while all three isoforms are ubiquitously expressed in proprioceptors, the relative levels differ, with $Na_V1.1$ having the most consistent level of expression across neurons analyzed. Furthermore, the average integrated density of the $Na_V1.1$ signal for a given proprioceptive DRG neuron was significantly higher than both $Na_V1.6$ and $Na_V1.7$ (**Fig 2E**, $p < 0.0001$).

Due to the ubiquitous expression of $Na_V1.1$, $Na_V1.6$, and $Na_V1.7$ in proprioceptors, we sought to determine the relative contributions of these isoforms to the proprioceptor whole-cell sodium current (I_{Na}). We performed *in vitro* voltage-clamp experiments on TdTomato+ neurons harvested from thoracic spinal levels of adult *Pvalb*^{Ai14} mice (de Nooij et al., 2013) and used serial application of selective Na_V channel antagonists to determine the specific contributions of $Na_V1.1$, $Na_V1.6$, and $Na_V1.7$ (**Fig 2F**). We first applied the selective $Na_V1.1$ antagonist ICA 1214314 (ICA, 500 nM), followed by 9-Anhydroustetrodoxin (AH-TTX, 300 nM), which is a selective $Na_V1.6$ blocker but also partially blocks $Na_V1.1$ (Denomme et al., 2020; Griffith et al., 2019). We reasoned that by first blocking the $Na_V1.1$ mediated current, the effect of AH-TTX should largely be due to inhibition of $Na_V1.6$. Finally, we blocked $Na_V1.7$ channels using the antagonist PF-05089771 (25 nM), followed by tetrodotoxin (TTX, 300 nM) to block any residual current, as proprioceptors do not express TTX-resistant Na_Vs. On average, 7.8% of the current remained unblocked following serial application of these antagonists due to incomplete block by the drugs used. We found that the ICA-sensitive component of I_{Na} was 44.8% of the total current. Conversely, 14.5% and 32.9%

of I_{Na} was sensitive to AH-TTX and PF-05089771, respectively (**Fig 2G**). No significant effect of the 0.1% DMSO vehicle solution on I_{Na} amplitude was observed (**Fig 2 – figure supplement 1**). Collectively, these data suggest that in proprioceptors $Na_V1.1$ is a dominant functional Na_V subtype.

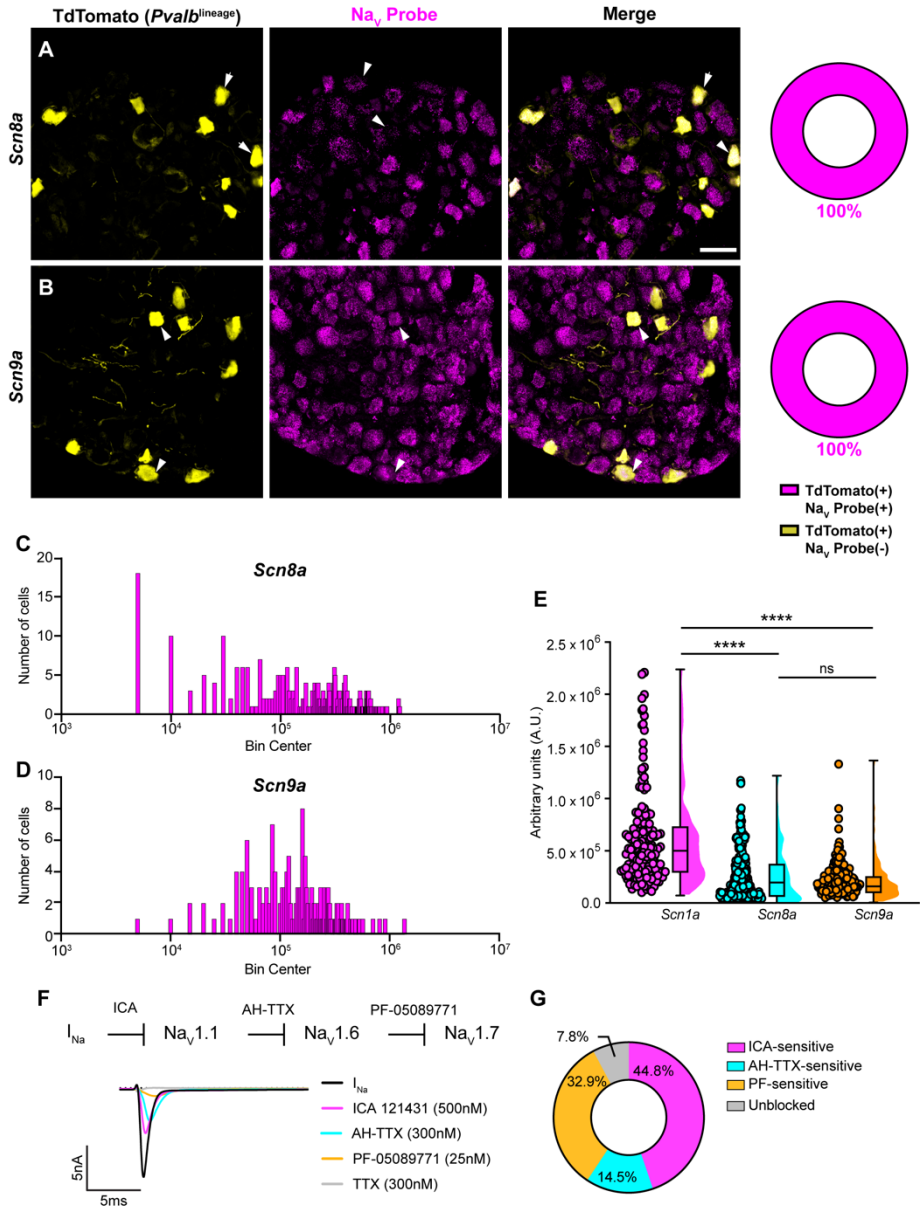

Figure 2. Transcriptomic and functional expression of sodium channels in proprioceptors. A-B. Representative confocal images of cryoprotected adult DRG sections (25 μm) with quantifications indicating the percentage of Na_V+ and Na_V- neurons in TdTomato+ proprioceptors. Sections were hybridized using RNAscope with probes targeting $Na_V1.6$ or $Na_V1.7$ (*Scn8a* and *Scn9a*, respectively, magenta) and stained with anti-DsRed (yellow). (**A**) *Snc8a*, n=298, (**B**) *Scn9a*, n=166. Scale bar set to 50μm. White arrowheads indicate Na_V+ neurons. **C-D.** Frequency distribution plots of integrated fluorescence density of $Na_V1.6$ and $Na_V1.7$ mRNA in TdTomato+ proprioceptors, respectively. **E**. The

average integrated density of *Scn1a*, *Scn8a*, and *Scn9a* RNAscope probe signal. Dots represent individual cells. Statistical significance was determined using a Kruskal-Wallis test with Dunn's post hoc comparisons. **F.** Top, experimental workflow of serial pharmacological blockade of Na_V channels expressed in proprioceptors. We first elicited a whole-cell sodium current in the absence of drug. We next bath applied 500nM of ICA 121431 to block current carried by $Na_V1.1$. Subsequently, we bath applied AH-TTX (300nM) to block $Na_V1.6$ mediated current, and PF-05089771 (25nM) to block the $Na_V1.7$ mediated current. Finally, TTX (300nM) was used to block residual current and to confirm there was no contribution of TTX-resistant Na_Vs in proprioceptors. Bottom, representative current traces following application of Na_V selective inhibitors. All drugs were applied for 1 minute. (**G**) Quantification of the average percentage of the whole-cell sodium current that was sensitive to the individual drugs used (n=8). n = cells. ****p<0.0001.

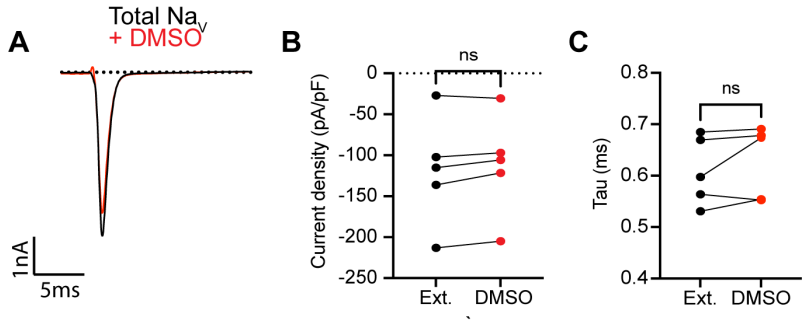

Figure supplement 1. 0.1% DMSO vehicle does not change I_{Na} in proprioceptors. (**A**) Representative current trace before (black trace) and after (red trace) application of 0.1% DMSO to TdTomato+ proprioceptors during *in vitro* electrophysiological experiments. Quantification of current density (**B**) and current decay kinetics (**C**) before (normal external solution) and after DMSO application. A paired t-test was used to determine statistical significance (p = 0.0855, n = 5 cells).

We next determined the biophysical features of the whole-cell sodium current (I_{Na}) in proprioceptors, which has not been previously reported (**Fig 3A-D**). The current-voltage relationship shows the first detectable current appeared at voltages near -50 mV and was maximal at voltages near -30 mV when evoked from a holding potential of -90 mV (**Fig 3B**). Voltage dependence of peak conductance was best fit to a single Boltzmann function and the voltage for half maximal activation was -38.7 mV (**Fig 3C**). The voltage-dependence of inactivation was determined with 40 ms prepulse steps ranging from -120 mV to +10 mV. The midpoint of the inactivation curve was -64.5 mV and was best fit to a single Boltzmann function (**Fig 3D**). To analyze recovery from fast inactivation, TdTomato+ neurons were depolarized to -20 mV, followed by a series of recovery periods ranging from 0.5 ms to 10 ms before a second test step to -20 mV was given to assess sodium channel availability. I_{Na} recovery was rapid (τ = 0.54 ms), with greater than 50% of I_{Na} recovered after 0.5 ms (**Fig 3E**). Finally, entry intro slow inactivation was determined. Cells were held at 0 mV during conditioning voltage steps ranging from 10 ms to 2000 ms, separated by two 2-ms pulses to -20 mV to compare channel availability before and

after the conditioning pulse (**Fig 3F**). The tau for entry into slow inactivation was 928.6 ms, with more than 50% of channels available after a 2000 ms conditioning pulse.

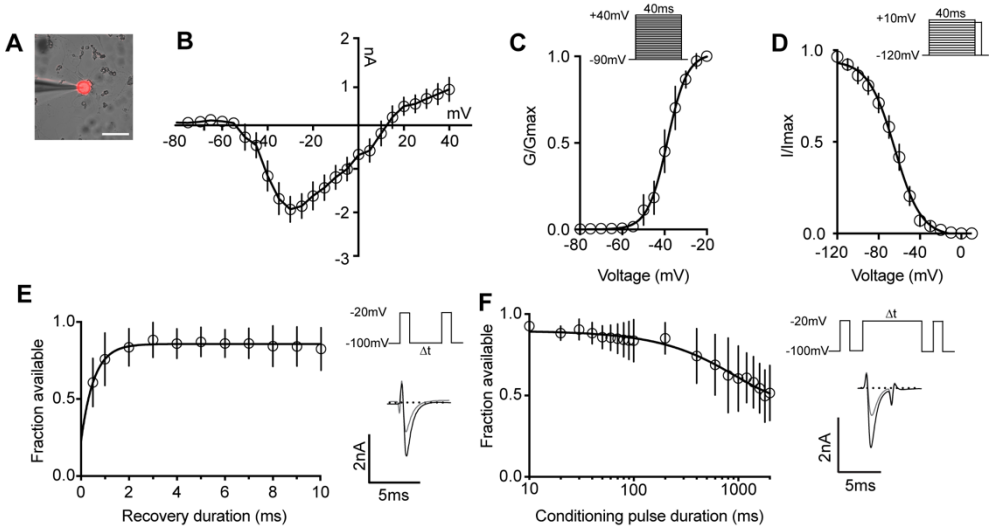

Figure 3. Biophysical analysis of the whole-cell sodium current (I_{Na}) in genetically identified proprioceptors. **(A)** Representative image of a TdTomato+ proprioceptor in culture during electrophysiological recordings (scale bar set to 50μm). **(B)** Current-voltage relationship of I_{Na} from TdTomato+ proprioceptors. Currents were elicited by 40 ms voltage steps from -90 mV to +40 mV in 5 mV increments (n=7-9). (**C**) Top, the voltage protocol used to measure the voltage dependence of for whole-cell sodium current activation in proprioceptors. Currents were elicited using a series of 40 ms voltage steps from -90 mV to 40 mV at 5 mV increments from a holding potential of -90 mV. Data are expressed as conductance over maximum conductance (n=6-9). (**D**) Top, the voltage protocol used to measure the voltage dependence of inactivation. A 40 ms prepulse ranging from -120mV to +10mV was given followed by a test pulse to 0 mV. Data are expressed as current over maximum current (n=8-12). (**E**) Left, quantification of recovery from fast inactivation (n=8). Line shows a monoexponential fit of the data (τ=0.54 ms). Top right, voltage-protocol to measure recovery from fast inactivation. A 20 ms step to -20 mV from -100 mV is followed by varying durations of recovery at -100 mV before a second test step to -20 mV. Bottom right, representative traces of currents elicited before (black trace) and after (grey trace) a 0.5 ms recovery period. (**F**) Left, quantification of entry into slow inactivation (n=6). Line shows a monoexponential fit of the data (τ=928.6 ms). Top right, voltage-protocol to measure entry into slow inactivation. A 3 ms test pulse to -20mV from -100mV was followed by conditioning pulses at 0 mV for varying durations before a third test step to -20mV. 12 ms recovery periods after the first test pulse and before the second were included to remove fast inactivation. Bottom right, representative current trace elicited before and after a 2000 ms conditioning pulse. n = cells.

We next asked how blocking $Na_V1.1$ channels affects proprioceptor function *in vitro*. Similar to serial pharmacological experiments, I_{Na} density in proprioceptors was significantly reduced from ~-140 pA/pF to ~-75 pA/pF following ICA application (**Fig 4B,** p = 0.0003). The proprioceptor I_{Na} had an average tau of 0.6 ms, which was significantly slowed to 1.0 ms following application of ICA (**Fig 4C,** p = 0.0007), in line with loss of a fast gating channel. Blocking $Na_V1.1$ did not change I_{Na} rise time (**Fig 4D,** p = 0.1611). Quantification of the ICA-sensitive component found an average tau of 0.4 ms and an average current density of -96 pA/pF (**Fig 4E**). Of note, there was a wide distribution of current densities for the ICA-sensitive component, ranging from

~-28 pA/pF to ~-263 pA/pF, suggesting some variability in the contribution of $Na_V1.1$ to proprioceptor excitability that may be proprioceptor subtype dependent. We next used current clamp experiments to determine the effect of ICA on proprioceptor intrinsic excitability (**Fig 4F**). Pharmacological inhibition of $Na_V1.1$ significantly reduced the number of evoked action potentials in most genetically identified proprioceptors (**Fig 4G**); however, 5 of the cells recorded had low firing rates that were not inhibited by ICA. This further suggests $Na_V1.1$ is important for repetitive firing in most proprioceptors, but some subtypes with lower intrinsic excitability instead rely on a combination of $Na_V1.6$ and $Na_V1.7$. Action potential amplitude (**Fig 4H**, p = 0.0420) and action potential threshold (**Fig 4I**, p = 0.0186) were also significantly reduced following ICA application, and action potential full-width half-max was significantly increased following ICA application (**Fig 4K**, p = 0.0068), in line with loss of the fast $Na_V1.1$-mediated current.

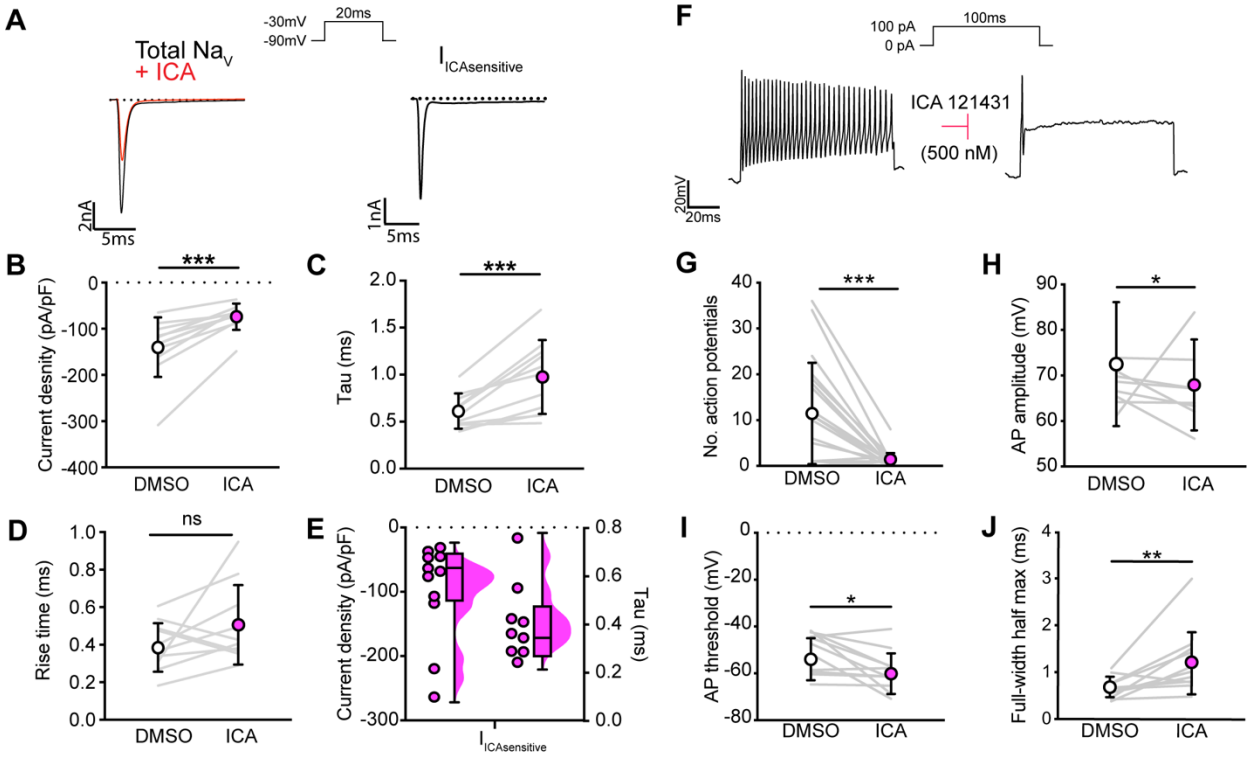

Figure 4. $Na_V1.1$ significantly contributes to the whole-cell sodium current and intrinsic excitability in genetically identified proprioceptors. A. Left, representative whole-cell voltage-clamp traces elicited before (black) and after (red) application of ICA121431 (500nM). Right, the subtracted ICA-sensitive current shown in black. **B.**

Quantification of the reduction in whole-cell current density before (white) and after (magenta) ICA, p = 0.0003, n=11 cells. **C.** Quantification of rate of current decay before and after ICA, p = 0.0007, n=11 cells. **D.** Quantification of whole-cell current rise time before and after ICA, p = 0.1611, n=10 cells. **E.** Left, current densities of ICA-sensitive sodium currents (n=11), right, current decay taus of ICA-sensitive sodium currents (n=9 cells). **F.** Representative whole-cell current clamp traces before (left) and after (right) application of ICA. **G-J,** Quantification of number of action potentials in response to current injection (**G,** p = 0.0002, n=20 cells), action potential amplitude (**H,** p = 0.0420, n=20 cells), action potential threshold (**I,** p = 0.0186, n=20 cells), and full-width half max (**J,** p = 0.0068, n=20 cells). Grey lines represent paired observations, circles and lines represent means and standard deviations. White circles, before ICA application. The Wilcoxon matched-pairs signed rank test was used to determine statistical significance.

It is important to note that ICA 121431 also blocks $Na_V1.3$ channels, which could be upregulated in our cultured DRG neuron preparations (Wangzhou et al., 2020). Indeed, a small but significant decrease in I_{Na} was observed in recordings from large-diameter DRG neurons harvested from *Pirt*^{Cre};Scn1a-floxed mice (Scn1a-cKO), which lack $Na_V1.1$ in all sensory neurons. Thus, inhibition of upregulated $Na_V1.3$ channels could contribute to the effect of on ICA on the proprioceptor I_{Na} **(Fig 4 - figure supplement 2)**.

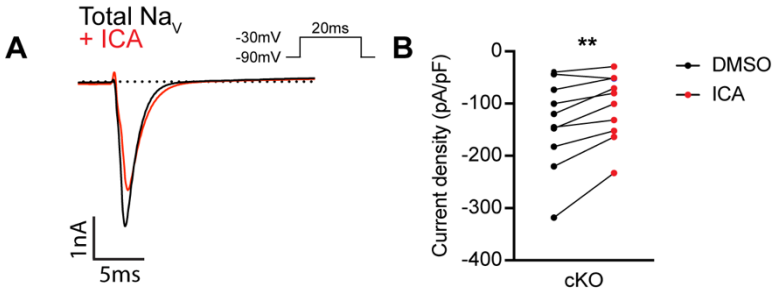

Figure supplement 2. ICA121431 may inhibit upregulated Nav1.3 channels in cultured DRG neurons. (**A**) and Representative whole-cell current trace from a large diameter DRG neurons (>60pF) from a Scn1a-cKO mouse. The black trace represents the I_{Na} recorded in external solution and the red trace represents the current following application of 500nM of ICA121431 for 1 minute. (**C**) Quantification of the current density before and after ICA (n=9). A significant effect of ICA was found (Paired student's t test, p = 0.0041). n = cells.

To clarify the importance of $Na_V1.1$ to proprioceptor function and avoid the caveats associated with *in vitro* pharmacological studies, we took an *in vivo* approach and analyzed motor behaviors in Scn1a-cKO mice of both sexes. We were precluded from using a *Pvalb*^{cre} driver line to directly interrogate a role for $Na_V1.1$ in proprioceptors, as loss of $Na_V1.1$ in Pvalb-expressing brain interneurons produces an epilepsy phenotype that prevents behavioral analyses in adult animals (Ogiwara et al., 2007). Consistent with *in vitro* data, Scn1a-cKO animals of both sexes displayed profound and visible motor abnormalities. These abnormalities include ataxic-like

tremors when suspended in the air (**Fig 5** - **video 1**), abnormal limb positioning (**Fig 5 -videos 2-3**), and paw clasping, which are absent in Scn1a-floxed littermate controls and heterozygous animals (*Pirt*^{Cre};*Scn1a*$^{fl/+}$, Scn1a-Het, respectively, **Fig 5A**). We first ran animals in the open field test for ten minutes each to quantify spontaneous locomotor behaviors (**Fig 5B**). We found that Scn1a-cKO animals traveled significantly less (**Fig 5C**) and slower (**Fig 5D**) than Scn1a-floxed littermate controls ($p = 0.0077$ and 0.0057, respectively). Surprisingly, Scn1a-Het mice also displayed motor abnormalities in the open field test, performing similarly to Scn1a-cKO animals (**Fig 5B-D**), demonstrating $Na_V1.1$ haploinsufficiency in sensory neurons for motor behaviors. No genotype-dependent differences were observed in the amount of time spent moving, suggesting gross motor function was intact (**Fig 5E**). Additionally, the amount of time spent in the center of the open field chamber was also independent of genotype (**Fig 5F**). We next used the rotarod assay to investigate differences in motor coordination. Mice were assayed on three consecutive days and latency-to-fall and RPM were quantified. Unlike in the open field assay, both Scn1a-floxed and Scn1a-Het mice performed at similar levels during the three-day period (**Fig 5G-H**). Conversely, Scn1a-cKO animals performed significantly worse. By day 3, on average they were only able to maintain their position on the rotarod for 41 s, falling over 50% faster Scn1a-floxed and Scn1a-Het mice. We did not observe any sex dependent differences in performance in the open field or rotarod tests (**Fig 5 - figure supplement 3**). We confirmed that our mouse model selectively targeted sensory neurons by crossing a *Pirt*^{Cre} driver with a fluorescent reporter line (*Pirt*^{Cre};*Rosa26*^{Ai14}). We observed little-to-no neuronal expression of TdTomato in both dorsal and ventral spinal cord (**Fig 5 - figure supplement 4**). In contrast, DRG somata and axons showed strong labeling. Collectively, our behavioral data provide evidence for a new *in vivo* role of $Na_V1.1$ in sensory neurons in mammalian proprioception.

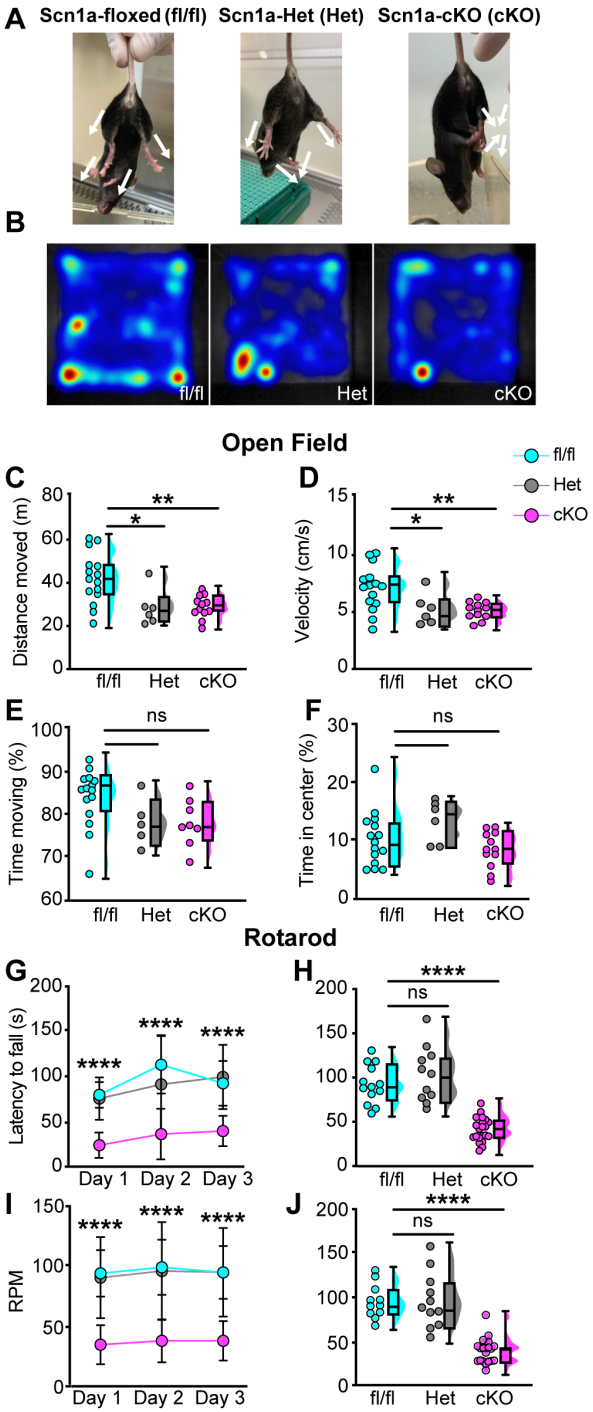

Figure 5. Loss of $Na_V1.1$ in peripheral sensory causes deficits in motor behaviors. A. Representative images showing limb positions of adult Scn1a-floxed (left), Scn1a-Het (middle), and Scn1a-cKO (right) mice. White arrows represent the direction of limbs. **B.** Representative heat maps from open field experiments between Scn1a-floxed (left), Scn1a-Het (middle), and Scn1a-cKO (right). Open Field (**C-F**), Quantification of total distance traveled during a 10-minute open-field test between Scn1a-floxed (cyan), Scn1a-Het (grey), and Scn1a-cKO (magenta) mice (**C,** Scn1a-Het p = 0.0255, Scn1a-cKO, p = 0.0077, compared to Scn1a-floxed,), average animal velocity (**D,** Scn1a-Het p = 0.00311, Scn1a cKO, p = 0.0057, compared to Scn1a-floxed), percent time moving (**E,** Scn1a-Het p = 0.1362, , p = 0.0730, compared to Scn1a-floxed), and percent time spent in center (**F,** Scn1a-Het p = 0.2297, Scn1a-cKO, p = 0.2494,

compared to Scn1a-floxed) during the test. Rotarod (**G-I**), Quantification of the latency to fall across three consecutive training days (**G**) and the day-three (**H**). Quantification of revolutions per minute (RPM) at the moment of animal fall (**I**) and the day-three average (**J**). Each dot represents one animal. ****p < 0.0001. A one-way ANOVA (Dunnett's post hoc comparison) was used to determine statistical significance in **C-F** and **I** and **J**. A two-way mixed-design ANOVA (Dunnett's post hoc comparison) was used to determine statistical significance in **G** and **H.** Open field: Scn1a-floxed N=15, Scn1a-Het N=6, Scn1a-cKO N=12. Rotarod: Scn1a-floxed N=11, Scn1a-Het N=11, Scn1a-cKO N=20.

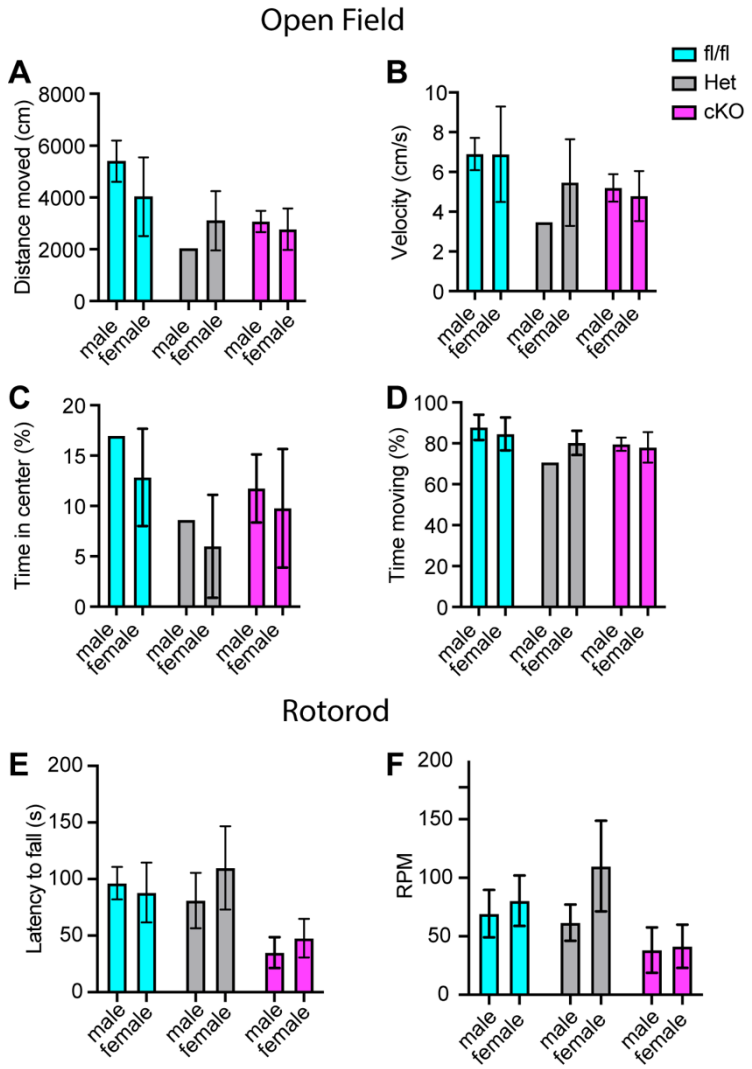

Figure supplement 3. Motor deficits in Scn1a-Het **and** Scn1a-cKO **animals are not sex dependent. A-D**. Quantification of sex-dependent parameters during a 10-minute open field trial. Total distance moved (**A**). Velocity (**B**). Percent time spent in center of box (**C**). Total percent time moving (**D**). Quantification of the sex-dependent differences in rotarod day-three trial latency to fall (**E**) and RPM (**F**).

320

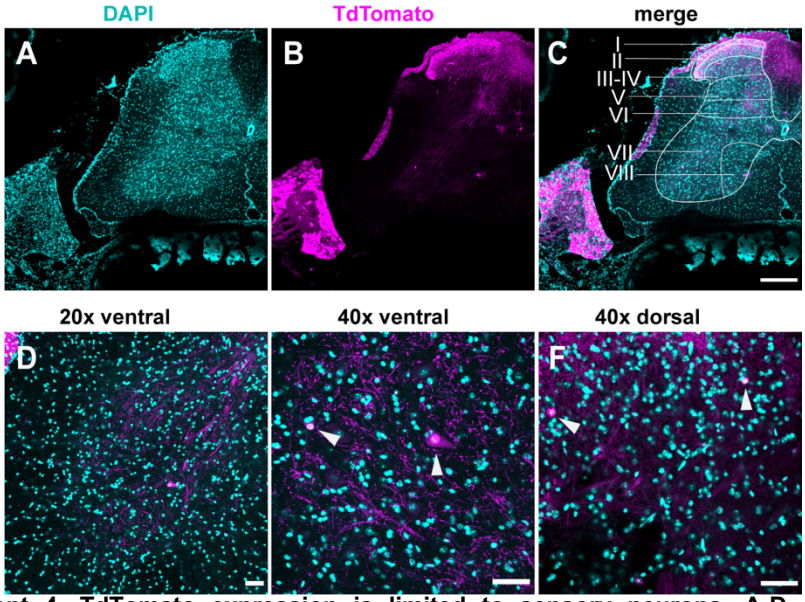

321 **Figure supplement 4. TdTomato expression is limited to sensory neurons. A-D**, Images stained using
322 immunohistochemistry with anti-DsRed (TdTomato) (**A-C**) Representative confocal images of spinal cord sections at
323 10X, 0.45 NA dry objective. Scale bar 200μm. (**D**) Image was taken at 20X, 0.8 NA dry objective of the ventral horn.
324 (**E**) Image was taken at 20X, 0.8 NA dry objective of the dorsal horn. Scale bar 50μm. (**F**) Image was taken at 40X, 1.3
325 NA oil-immersion objective. Arrows indicate TdTomato+ puncta. Scale bar 50μm. (N=3, n=30 sections).
326
327

328

Video 1. Uncoordinated movements in Scn1a-cKO **animals.** A Scn1a-cKO mouse (left) shows abnormal and spastic movements when suspended in the air. These movements are absent in Scn1a-floxed mice (right).

Video 2. Abnormal limb position in Scn1a-cKO **animals.** A Scn1a-cKO mouse has uncoordinated leg movements and makes an abnormal rotation of its hind paw to grasp its tail while suspended in the air.

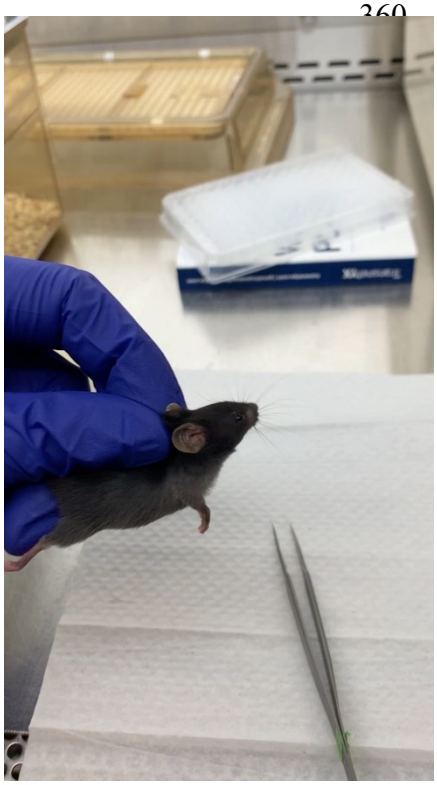

Video 3. Abnormal paw position in Scn1a-cKO **animals.** A Scn1a-cKO mouse is scruffed and places hind paws with foot pads facing down. This contrasts with the normal paw positioning seen in the forepaws, in which foot pads are in the outward facing position.

Could the motor deficits observed in Scn1a-cKO mice be due to abnormal proprioceptor development? To address this question, we performed RNAscope analysis of DRG sections from Scn1a-floxed, Scn1a-Het, and Scn1a-cKO mice. We quantified the number of neurons per DRG section that were positive for both *Runx3* and *Pvalb* transcript, the molecular signature of mature proprioceptors (**Fig 6**, Oliver et al., 2021). We found no significant genotype-dependent differences in the number of proprioceptors in Scn1a-Het and Scn1a-cKO mice compared to Scn1a-floxed controls ($p = 0.3824$ and $p = 0.1665$, respectively), indicating that the behavioral deficits observed in Scn1a-cKO mice are not the result of a developmental loss of proprioceptors. We also analyzed muscle spindle morphology to determine if aberrant sensory end organ development may contribute to the observed motor abnormalities. Similar to conditional Piezo2-knockout animals (Woo et al., 2015), no qualitative differences were observed between genotypes (**Fig 6 - figure supplement 5**). Thus, abnormal proprioceptor development does not contribute to the overall phenotype of Scn1a-cKO mice.

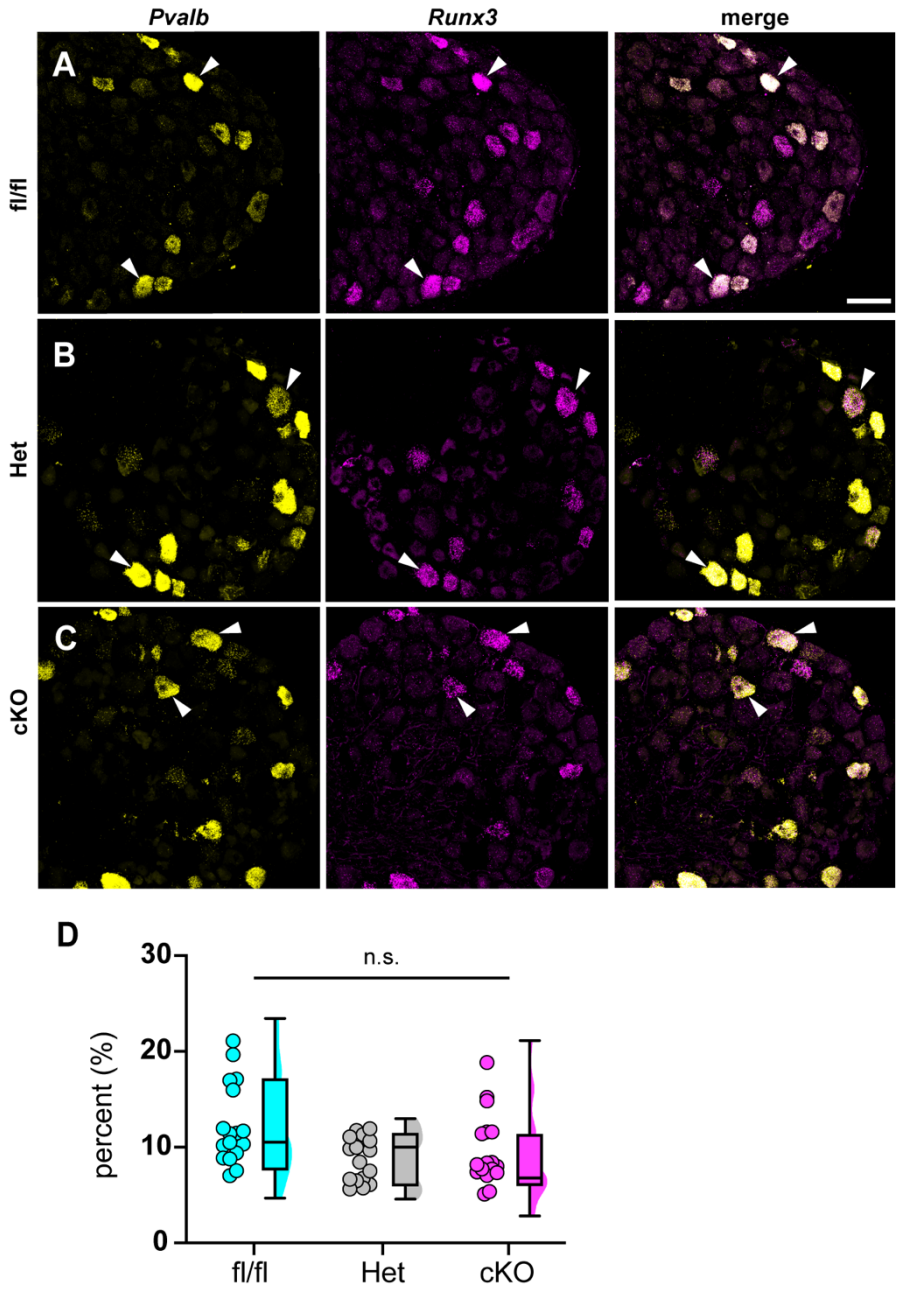

Figure 6. Loss of $Na_V1.1$ in sensory neurons does not affect proprioceptor development. Representative images of Scn1a-floxed (**A**), Scn1a-Het (**B**), and Scn1a-cKO (**C**) adult DRG neuron sections (25 μm). Images were acquired with a 40X, 0.9 NA water-immersion objective. Sections were hybridized with probes targeting parvalbumin (*Pvalb*, yellow) and *Runx3* (magenta). (**D**) Quantification of the percentage of Pvalb+/*Runx3*+ neurons in each genotype. Each dot represents one DRG section. A Kruskal-Wallis test with Dunn's post hoc comparison was used to determine statistical significance (p = 0.1971, Scn1a-floxed n=17, Scn1a-Het n=17, Scn1a-cKO n=18)). Scale bar 50μm.

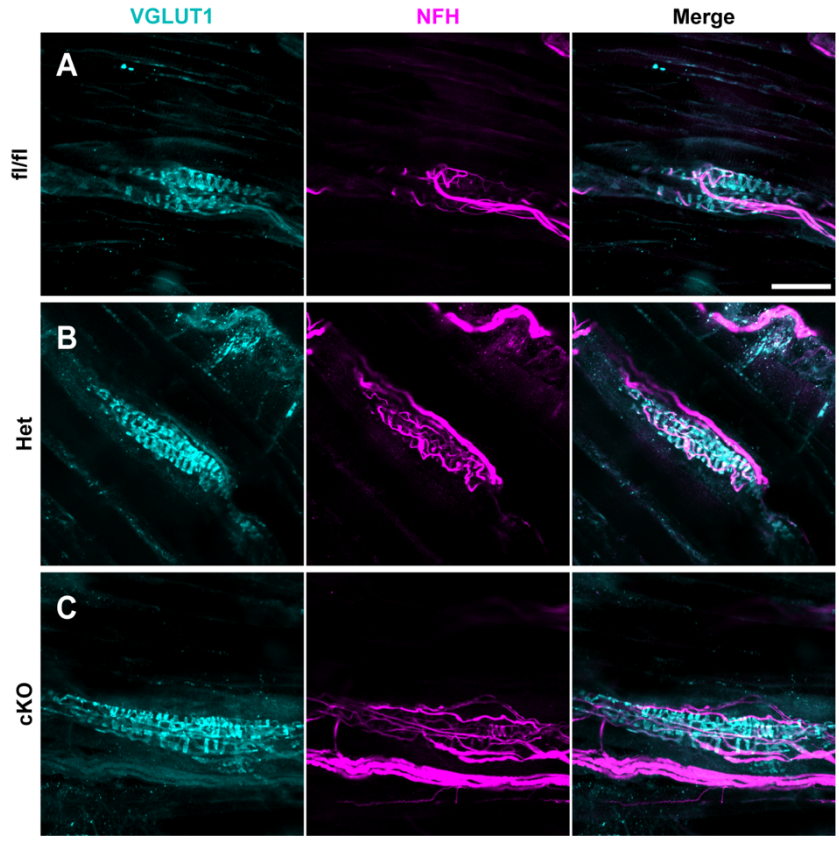

Figure supplement 5. Muscle spindle development is normal in Scn1a-Het **and** Scn1a-cKO **animals**. **A-C**, Representative confocal images of muscle spindle whole mounts. Images were acquired with a 40x, 1.3 NA oil-immersion objective. Sections were stained using immunohistochemistry with VGLUT1 (cyan) and neurofilament heavy (NFH, magenta). (**A**) Representative images from Scn1a-floxed (**B**) Scn1a-Het and (**C**) Scn1a-cKO mice. Scn1a-floxed, n=7; Scn1a-Het, n=8; Scn1a-cKO, n=9. Scale bar 50μm. n = muscle spindles.

We next asked whether the motor deficits of Scn1a-cKO mice are due to altered synaptic connectivity between proprioceptive axons and motor neurons in the ventral spinal cord. Spinal cord sections were harvested from Scn1a-floxed, Scn1a-Het, and Scn1a-cKO mice and stained with antibodies against vesicular glutamate transporter 1 (VGLUT1) to label proprioceptor axons, and choline acetyltransferase (ChAT). ChAT primarily labels α- and γ-motoneurons in the ventral horn, which can be distinguished based on size. We analyzed the number of VGLUT1 puncta on the somata and proximal dendrites of individual cholinergic neurons greater than 400 μm^2 to bias our quantification towards α-motorneurons. We found no significant decrease in VGLUT puncta density per ChAT+ neuron between Scn1a-Het or Scn1a-cKO when compared to Scn1a-floxed

404 littermate controls (**Fig 7,** Scn1a-Het, p>0.9999, Scn1a-cKO, p=0.4573). This suggests that
405 general deficits in proprioceptor innervation of motor neurons do not contribute to the phenotype
406 of Scn1a-cKO mice.
407

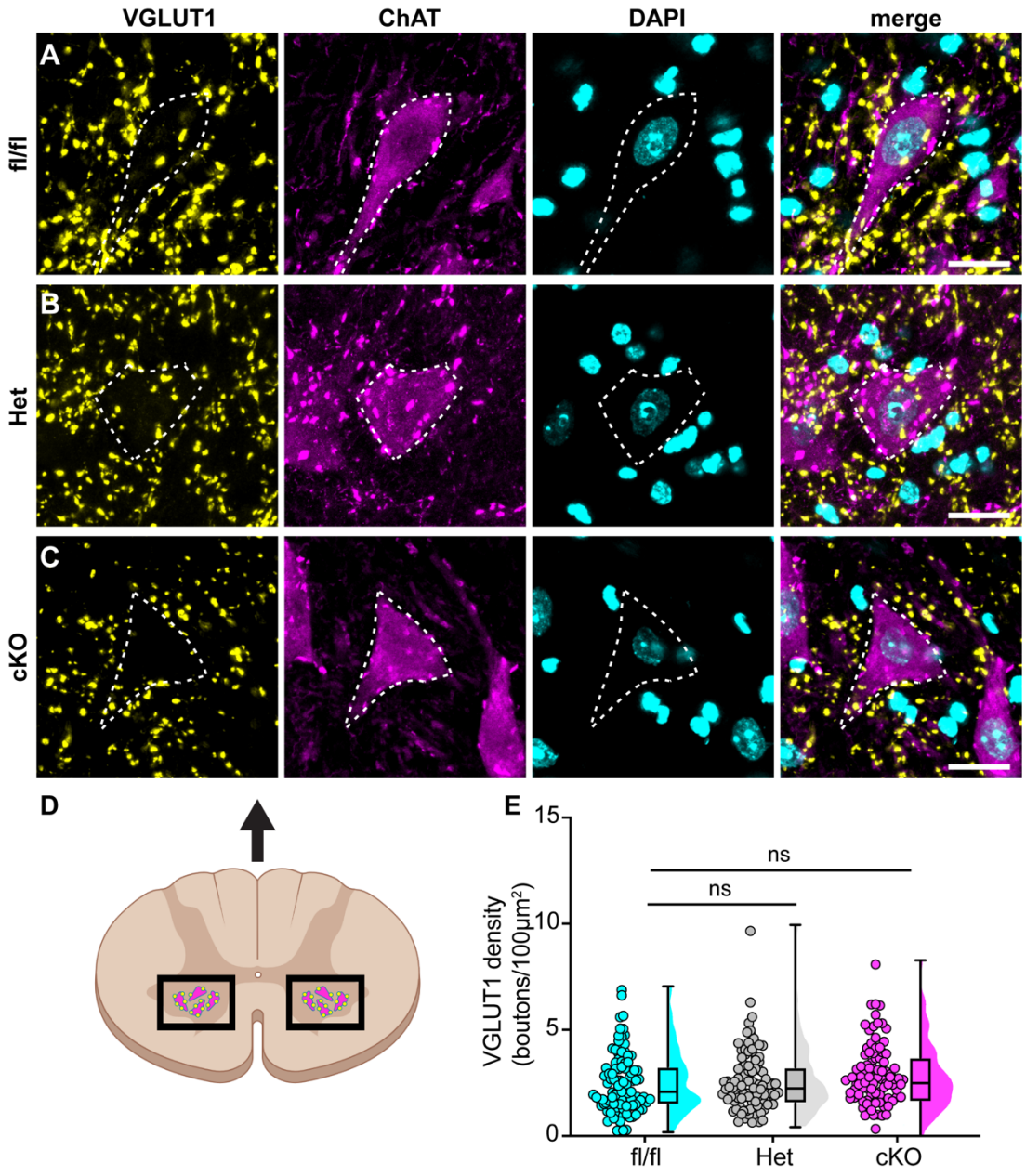

408

409 **Figure 7. Loss of $Na_V1.1$ in sensory neurons does not change proprioceptor innervation of α-motoneurons**. **A-**
410 **C**, Representative images of Scn1a-floxed(**A**), Scn1a-Het (**B**), and Scn1a-cKO (**C**) adult spinal cord sections (30 μm).
411 Images were acquired with a 63X, 1.4 NA water-immersion objective. Sections were stained using immunochemistry

with VGLUT1 (yellow) and ChAT (magenta). Nuclei (cyan) were labeled with DAPI. (**D**) Schematic of spinal cord regions of interest. (**E**) Quantification of the average density of VGLUT1+ puncta per 100μm^2 onto ChAT+ neurons that were larger than 400μm^2. A Kruskal-Wallis test with Dunn's post hoc comparison was used to determine statistical significance Each dot represents a motor neuron. Scn1a-floxed, n=101; Scn1a-Het, n=102; Scn1a-cKO, n=92. Scale bar 20μm. n = cells.

We next asked whether proprioceptor electrical signaling is altered in Scn1a-cKO mice. While *in vitro* patch-clamp electrophysiology can assess Na_V function at DRG somata and provide insight as to how they contribute to intrinsic excitability, the physiological contributions of ion channels in DRG soma to somatosensory transmission *in vivo* are not well understood. Thus, to directly investigate how $Na_V1.1$ shapes action potential propagation down proprioceptor axons, we used an *ex vivo* preparation to recording muscle afferent activity during ramp-and-hold stretch and sinusoidal vibration. Afferents from both Scn1a-Het and Scn1a-cKO mice exhibited impaired static stretch sensitivity as evidenced by a decreased likelihood of firing during rest as compared to Scn1a-floxed mice, as well as an inability to maintain firing throughout the entire 4s stretch. Almost all afferents from Scn1a-floxed mice could fire consistently throughout the entire 4s hold phase (**Fig 8A**), but loss of one or both copies of $Na_V1.1$ led to either firing only near the beginning of stretch or inconsistent firing in a high percentage of afferents lacking $Na_V1.1$ (**Fig 8B,C**). We quantified this inconsistent firing by determining the coefficient of variation (CV) of the interspike interval (ISI) during the plateau phase of stretch (1.5-3.5 s into the hold phase) across different stretch lengths and found a significant effect of genotype, with the knockout afferents both having higher ISI CV than the Scn1a-floxed afferents (**Fig 8D**; 0.074 $\pm$ 0.06, 0.313 $\pm$ 0.456, .497 $\pm$ .831, at 7.5% Lo, Scn1a-floxed, Scn1a-Het, and Scn1a-cKO afferents, respectively, Two-way ANOVA, main effect of genotype, p = 0.015). In contrast to the clear deficits in static sensitivity in afferents lacking $Na_V1.1$, dynamic sensitivity was not significantly impaired. The maximum firing frequency during the ramp up phase (Dynamic Peak) was independent of genotype, and even trended slightly higher in afferents lacking $Na_V1.1$ (**Fig 8E**; Two-way ANOVA, effect of genotype p=0.0633).

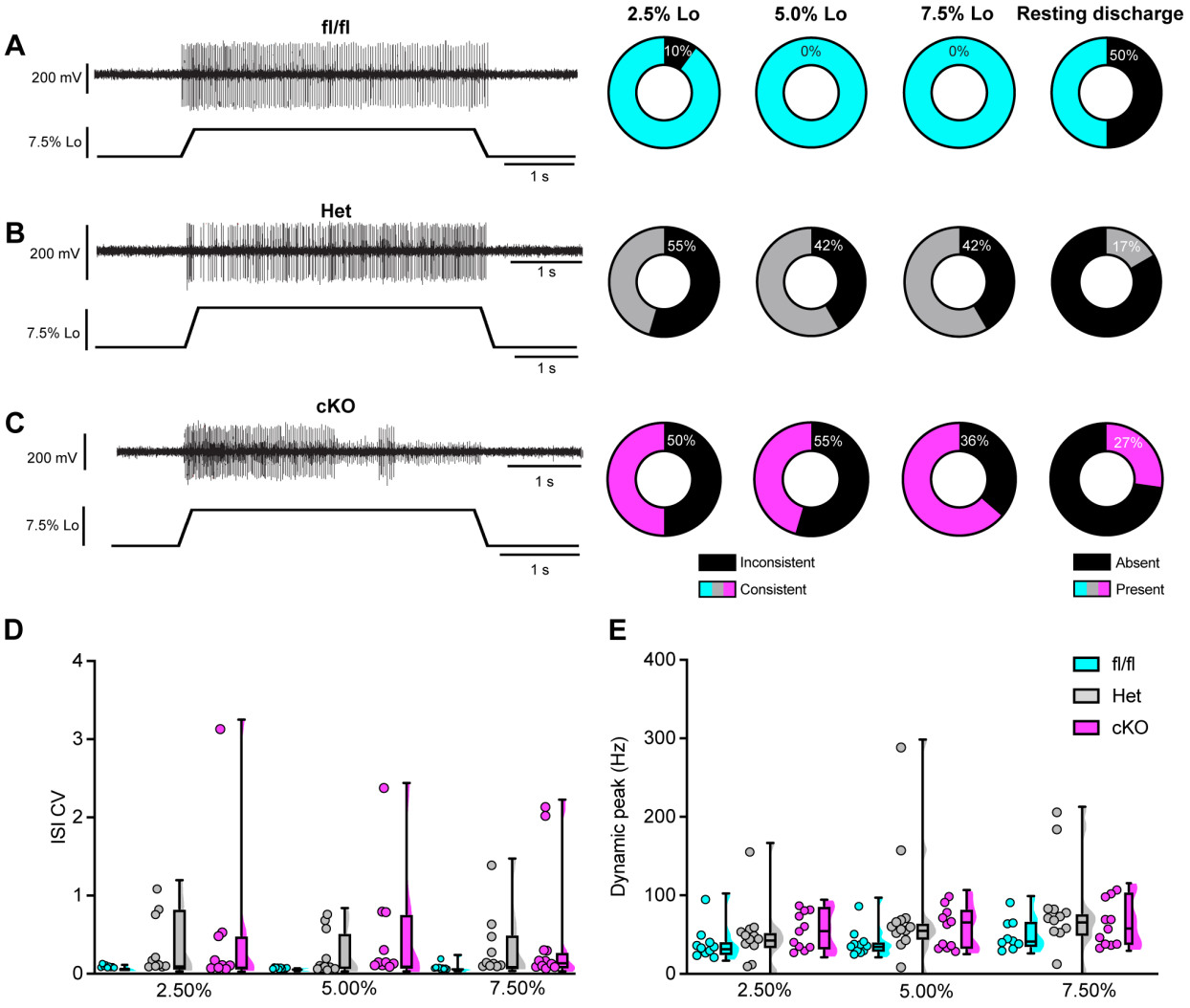

Figure 8. Loss of $Na_V1.1$ reduces static muscle stretch sensitivity and reliability. A-C. Representative responses to ramp-and-hold muscle stretch at 7.5% of optimal length (Lo) from Scn1a-floxed (**A**), Scn1a-Het (**B**) and Scn1a-cKO (**C**) afferents. Afferents from Scn1a-Het and Scn1a-cKO mice were more likely to show inconsistent firing during the hold phase of stretch. The percentage of afferents from each genotype that were able to fire consistently for the entire duration of stretch at 2.5%, 5.0%, and 7.5% of Lo are shown in the pie charts next to the representative trace from their genotype (black indicates percentage with inconsistent firing). The final pie charts represent the proportion of afferents that exhibited resting discharge at Lo for every stretch for each genotype (black indicates absence of resting discharge). **D.** Inconsistency in firing was quantified as the interspike interval coefficient of variation (ISI CV) during the plateau stage of the hold phase of stretch (1.5-3.5s into stretch) for the 3 different genotypes. A significant effect of genotype was observed (two-way mixed-design ANOVA, p=0.015) **E.** The highest firing rate during the ramp up phase of stretch (dynamic peak) is a measure of dynamic sensitivity. No significant effect of genotype on dynamic peak was observed (two-way mixed-design ANOVA, p=0.0633). Each dot represents one afferent in **D** & **E** (Scn1a-floxed, n=10; Scn1a-Het, n=12; Scn1a-cKO, n=11).

We next examined the requirement of $Na_V1.1$ for proprioceptor afferent responses to sinusoidal vibration, which is a measure of dynamic sensitivity, and found no differences with loss

of $Na_V1.1$ (**Fig 9A-C, Tables 2-4**). We characterized a unit as having entrained to vibration if it fired at approximately the same time every cycle of the 9s vibration. In most cases, afferents lacking $Na_V1.1$ were equally likely to entrain to vibration than Scn1a-floxed afferents (**Fig 9D-F**). Indeed, Scn1a-cKO afferents were able to maintain firing during the entire 9 s sinusoidal vibration, in contrast to their inability to maintain consistent firing during 4 s of static stretch. There were no significant differences in firing rate during vibration between Scn1a-floxed, Scn1a-Het, and Scn1a-cKO afferents (**Fig 9D-F**). Taken together, our *ex vivo* recordings suggest that behavioral deficits in Scn1a-cKO result from abnormal proprioceptor responses to static muscle movement, whereas afferent responsiveness to dynamic stimuli is $Na_V1.1$-independent. Furthermore, recordings from Scn1a-Het animals support the notion that $Na_V1.1$ is haploinsufficient for proprioceptor function at the cellular level.

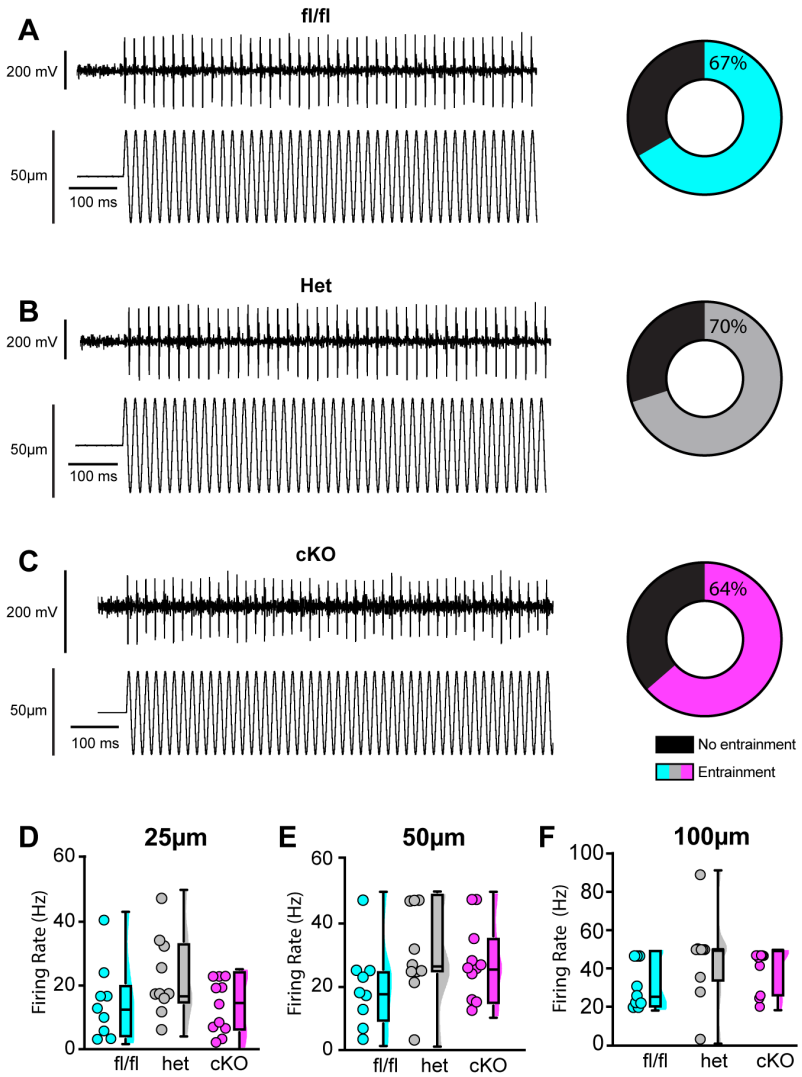

Figure 9. Loss of $Na_V1.1$ does not alter muscle spindle afferent response to vibratory muscle stretch. A-C. Representative traces from afferents that were able to entrain to a 50Hz, 100µm vibration as well as graphs with the percentage of all Scn1a-floxed (cyan; **A**), Scn1a-Het (gray; **B**), and Scn1a-cKO (magenta; **C**) afferents that could entrain to the vibration shown in **A-C**. Average firing frequency during a 9 s 50 Hz vibration shown for a 25 µm (**D**), 50 µm (**E**), and 100 µm (**F**) amplitude vibration. There was no significant effect of genotype on the firing frequency during vibration (25 µm, p = 0.2398, 50 µm, p = 0.2413, 100 µm, p = 0.1276). A one-way ANOVA was used to determine statistical significance in **D** and **E**. A Kruskal-Wallis test was used to determine statistical significance in **F**. Each dot represents one afferent (Scn1a-floxed, n=9; Scn1a-Het, n=10; Scn1a-cKO,n=11).

Table 2. Afferent entrainment to 25 µm amplitude vibration

Genotype	10 Hz	25 Hz	50 Hz	100 Hz
Scn1a-floxed	33.33%	11.11%	0.00%	0.00%
Scn1a-Het	50.00%	40.00%	10.00%	10.00%
Scn1a-cKO	27.27%	9.09%	0.00%	0.00%

Table 2. The percentage of muscle spindle afferents that entrained to a 25µm amplitude sinusoidal vibration.

Table 3. Afferent entrainment to 50 μm amplitude vibration

Genotype	10 Hz	25 Hz	50 Hz	100 Hz
Scn1a-floxed	88.89%	22.22%	11.11%	11.11%
Scn1a-Het	80.00%	70.00%	30.00%	10.00%
Scn1a-cKO	45.45%	54.55%	18.18%	0.00%

Table 3. The percentage of muscle spindle afferents that entrained to a 50μm amplitude sinusoidal vibration.

Table 4. Afferent entrainment to 100 μm amplitude vibration

Genotype	10 Hz	25 Hz	50 Hz	100 Hz
Scn1a-floxed	100.00%	44.44%	33.33%	22.22%
Scn1a-Het	90.00%	90.00%	70.00%	40.00%
Scn1a-cKO	63.64%	72.73%	63.64%	18.18%

Table 4. The percentage of muscle spindle afferents that entrained to a 100μm amplitude sinusoidal vibration.

DISCUSSION

The critical role for $Na_V1.1$ in various brain disorders has overshadowed the potential contributions of this channel in peripheral signaling. The results presented in this study are the first to provide functional evidence that $Na_V1.1$ in peripheral sensory neurons is required for normal proprioception. We found that mice lacking $Na_V1.1$ in sensory neurons exhibit visible motor deficits and ataxic-like behaviors, which we propose is largely attributed to loss of $Na_V1.1$ in proprioceptors. Indeed, RNAscope analysis showed expression of $Na_V1.1$ mRNA in 100% of genetically identified proprioceptors. While $Na_V1.6$ and $Na_V1.7$ were also ubiquitously expressed in proprioceptors, $Na_V1.1$ displayed higher expression levels, consistent with a previous RNAsequencing study (Zheng et al., 2019b). There are anywhere from 5 to 8 different proprioceptor molecular subclasses (Oliver et al., 2021b; Wu et al., 2021), however, and it is possible that these distinct classes rely on different combinations of these channels for function. Nevertheless, our functional *in vitro* patch-clamp experiments found $Na_V1.1$ to be the dominant subtype across recorded neurons, comprising nearly half of the proprioceptor I_{Na}. In line with this, pharmacological inhibition of $Na_V1.1$ is sufficient to significantly attenuate action potential firing is

most proprioceptors; yet, it should be noted that 25% of the neurons we recorded fired action potentials that were insensitive to ICA application. This suggests that some proprioceptor subtypes rely more heavily on $Na_V1.6$ and $Na_V1.7$ for electrical activity. Interestingly, the proprioceptors that were insensitive to ICA application also were less intrinsic excitable, firing only 1-2 action potentials in response to current injection, as opposed to the other 75% on neurons recorded, which fired repetitively during the 100 ms injection protocol. This further supports a role for $Na_V1.1$ in maintaining action potential firing in response to sustained stimulation. These results, however, should be interpreted with the caveat that in these experiments ICA may also be acting on $Na_V1.3$ channels that are upregulated during DRG neuron culturing (Wangzhou et al., 2020). Nevertheless, at the afferent level Scn1a-cKO and Scn1a-Het animals show clear deficits in static stretch sensitivity, but not dynamic sensitivity, and could even entrain to vibrations as fast as 100 Hz, suggesting a specific role for $Na_V1.1$ in proprioceptors responses to static muscle movement. Finally, we found that loss of $Na_V1.1$ in sensory neurons had no effect on proprioceptor development, muscle spindle morphology, or proprioceptive afferent innervation of ChAT+ motor neurons in the spinal cord. Thus, the observed motor behavioral deficits are likely due to reduced static sensitivity of proprioceptor afferents.

Our model proposes that $Na_V1.1$ is tasked with maintaining consistent firing in spindle afferents during static muscle stretch for normal motor behaviors, whereby activation of the mechanotransduction channel Piezo2 initiates electrical signaling, which in turn activates a complement of tetrodotoxin-sensitive Na_V channels (Carrasco et al., 2017; Florez-Paz et al., 2016; Woo et al., 2015, **Fig 10**). During dynamic or vibratory stimuli, Piezo2, and likely a combination of other molecular mediators, including $Na_V1.6$ and $Na_V1.7$, are sufficient to elicit normal electrical activity. Conversely, during prolonged muscle stretch when Piezo2 channels presumably inactivate, $Na_V1.1$ is required for regular and reliable firing. While other signaling molecules and channels, such as vesicle-released glutamate (Bewick et al., 2005; Than et al., 2021), and

529 mechanosensitive ASIC channels (Lin et al., 2016) and ENaC channels (Bewick and Banks,
530 2015), also contribute to mammalian proprioception, our data suggests $Na_V1.1$ is a critical for
531 muscle spindle afferent mechanotransduction, given the overt behavioral deficits observed in
532 Scn1a-cKO mice. Due to the ubiquitous expression of $Na_V1.1$ in all proprioceptors and the
533 importance of Golgi Tendon Organ (GTO) feedback to motor control, alterations in function in
534 those proprioceptors likely contribute to the behavioral deficits we observed; however, we did not
535 directly measure their function.

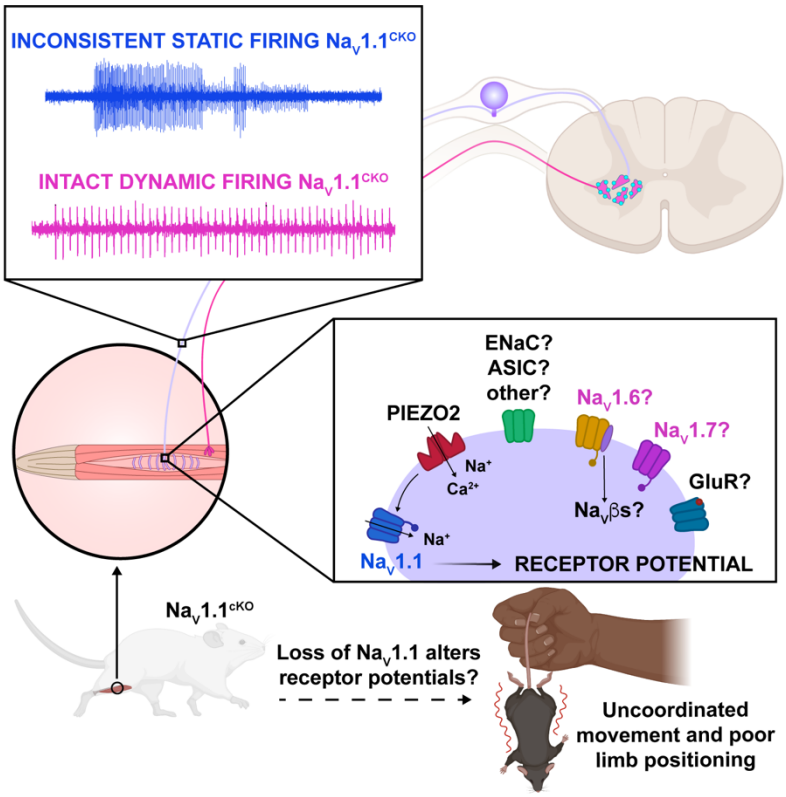

536

537 **Figure 10. Proposed model of the role of $Na_V1.1$ in proprioception.** Upon muscle static stretch, various channels
538 activate, including Piezo2 (red) which results in an influx of calcium and sodium ions, causing a depolarization that
539 activates $Na_V1.1$ (dark blue). $Na_V1.1$ activation drives reliable repetitive firing of proprioceptors during static stretch for
540 normal motor behavior. Loss of $Na_V1.1$ in sensory neurons results in inconsistent static firing at the afferent level while
541 maintaining dynamic firing, resulting in uncoordinated movements and abnormal limb positioning. It is possible that a
542 combination of Piezo2, $Na_V1.6$ (yellow), $Na_V1.7$ (pink), and/or other channels, such as glutamate receptors (dark blue),
543 ASIC and ENaC channels (green) mediate dynamic firing.
544

To date, our knowledge of the functional contributions of $Na_V1.1$ in the PNS is limited. Most studies have identified roles for this channel in mechanical pain signaling in DRG, TG, and vagal sensory neurons. Intraplantar pharmacological activation of $Na_V1.1$ induces spontaneous pain behaviors and mechanical pain, which is absent in mice lacking $Na_V1.1$ in small- and medium-diameter sensory neurons (Osteen et al., 2016b). Inhibition of $Na_V1.1$ prevented the development of mechanical pain in several preclinical models, including spared nerve injury (Salvatierra et al., 2018b), an irritable bowel syndrome mouse model (Salvatierra et al., 2018), and infraorbital nerve chronic constriction injury (Pineda-Farias et al., 2021). Additionally, blocking $Na_V1.1$ channels inhibited firing in TRPM8-expressing neurons *in vitro*, suggesting a potential role for this channel in thermosensation (Griffith et al., 2019). No prior studies, however, have reported a functional role for $Na_V1.1$, or Na_Vs in general, in proprioception.

The loss of consistent firing we observed during static stretch in Scn1a-cKO and Scn1a-Het animals is functionally similar to deletion of $Na_V1.1$ in other brain cell types. Indeed, loss of a single copy of $Na_V1.1$ is sufficient to attenuate sustained action potential firing in parvalbumin-positive hippocampal interneurons (Ogiwara et al., 2007; Yu et al., 2006) and cerebellar Purkinje neurons (Yu et al., 2006). $Na_V1.1$ has been associated with persistent sodium current ($I_{Na}P$) and resurgent sodium current ($I_{Na}R$), both of which promote repetitive firing in a wide variety of cell types in the CNS and PNS (Barbosa et al., 2015; Kalume et al., 2007; Khaliq et al., 2003). $Na_V1.1$ also recovers rapidly from fast inactivation compared to other channel subtypes (Herzog et al., 2003; Patel et al., 2015) and has been shown to be refractory to entry into slow inactivation in TRPM8-expressing DRG neurons (Griffith et al., 2019). We observed similar characteristics when analyzing the proprioceptor I_{Na}. Future studies will determine whether proprioceptors rely on these features of $Na_V1.1$ for reliable and consistent encoding of static muscle stretch.

Loss of $Na_V1.1$ notably impacted proprioceptor afferent static sensitivity during ramp-and-hold stretch, but not dynamic sensitivity as measured by entrainment to sinusoidal vibrations using *ex vivo* muscle-nerve recordings. Afferents from Scn1a-cKO animals were more likely to have

action potential failures and thus were largely unable to fire consistently throughout the 4 s of stretch, which was accompanied by a higher coefficient of variability in the ISI. This indicates that $Na_V1.1$ has a critical role in transmitting static stretch information to the central nervous system. Interestingly, however, dynamic sensitivity in these afferents appears to be unimpaired. Both Scn1a-cKO and Scn1a-Het afferents were able to entrain throughout the entire 9 s vibration; therefore, $Na_V1.1$ does appear to have a generalized role in maintaining high frequency firing, but a more specific deficit in static sensitivity. $Na_V1.1$ has been localized to muscle spindle afferent endings and has been hypothesized to help amplify receptor current (Carrasco et al., 2017) . Our results support a model whereby current from Piezo2 and potentially other mechanically sensitive ion channels at the start of stretch produces a sufficient receptor potential to generate firing at the heminode, but that amplification of the receptor potential by $Na_V1.1$ is necessary to maintain firing during held stretch.

A similar deficit in static but not dynamic sensitivity was seen following loss of synaptic-like vesicle released glutamate from afferent endings (Than et al., 2021); however in those afferents firing only occurred at the beginning of stretch and patchy firing was never observed. This may indicate that glutamate plays a more general role maintaining excitability, whereas $Na_V1.1$ is required for reliable action potential generation at heminodes during static stimuli. Alternatively, or in addition, $Na_V1.1$ expressed along the axon could be essential for sustained static firing. A detailed examination of $Na_V1.1$ subcellular localization along proprioceptor afferents could shed light on how this channel contributes to signal propagation. The lack of an effect on dynamic sensitivity could suggest the upregulation of other Na_V subtypes or other molecules as a compensatory mechanism to counteract the loss of $Na_V1.1$. Indeed, our *in vitro* electrophysiological experiments found a more pronounced effect of acute $Na_V1.1$ inhibition on proprioceptor excitability. This could be due, however, to artificially upregulated $Na_V1.3$ channel activity in culturing conditions, or conversely, a higher density of $Na_V1.1$ expression in

proprioceptor somata. Future studies using temporally controlled deletion of $Na_V1.1$ in sensory neurons could tease this apart. Nevertheless, as static sensitivity is still very much impaired in both Scn1a-cKO and Scn1a-Het afferents, $Na_V1.1$ may play a potentially unique role in maintaining afferent firing during the sustained stretch.

Loss of $Na_V1.1$ in sensory neurons did not impact proprioceptor development, as the number of proprioceptors in DRG sections was unchanged between genotypes, and muscle spindles developed normally in our model. While we did not directly examine GTOs, we do not anticipate that abnormal end organ development would be restricted to that proprioceptor subtype. Additionally, we did not observe a general decrease in α-motor neuron innervation, which is consistent with the findings of Mendelsohn et al., 2015, who reported loss of proprioceptor activity does not generally reduce proprioceptive input into the spinal cord. Interestingly, however, the authors did observe changes in heteronymous sensory-motor connectivity when proprioceptor transmission was blocked, whereby proprioceptor innervation of motor neurons that project to antagonistic muscles was increased. Whether loss of $Na_V1.1$ in proprioceptive afferents causes them to "mis-wire" in our model to make connections with inappropriate motor neuron pools is unclear. Future studies will determine if this contributes to the observed behavioral deficits.

We found effects of both pharmacological inhibition and genetic deletion of $Na_V1.1$ in *in vitro* and *ex vivo* electrophysiological experiments, respectively (**Figs 2-3, 8-9**); however, in our mouse model $Na_V1.1$ is deleted in all sensory neurons. Thus, we cannot rule out that loss of $Na_V1.1$ in other mechanosenory neuron populations, such as touch receptors, contributes to the motor deficits observed. Deletion of $Na_V1.1$ in small- and medium-diameter DRG neurons using a peripherin-Cre driver did not produce visible motor deficits (Osteen et al., 2016b), indicating sensory neuron populations in those categories are not involved. We did observe $Na_V1.1$ transcripts in the vast majority of myelinated DRG neurons (a combination of large- and medium-diameter DRG neurons), consistent with its presence in different subclasses of tactile sensory

neurons (Zheng et al., 2019). However, the severe motor phenotype of Scn1a-cKO mice precludes mechanical threshold analysis using von Frey or tactile sensitivity using tape test. Notably, baseline mechanical thresholds were unchanged following intraplantar injection of a selective $Na_V1.1$ inhibitor (Salvatierra et al., 2018). This suggests that while $Na_V1.1$ mRNA is expressed in most tactile sensory neurons, functional protein may only be upregulated in these populations during pathological states.

Despite this limitation, one noteworthy and intriguing finding from our study was the haploinsufficiency of $Na_V1.1$ in sensory neurons for proprioceptor function and normal motor behavior in the open field test. At the afferent level, heterozygous and homozygous loss of $Na_V1.1$ produced similar deficits in static firing, suggesting that loss of less than a quarter of the proprioceptor I_{Na} is sufficient to impair proprioceptor responsiveness to muscle stretch. $Na_V1.1$ is haploinsufficeint in several brain neuron cell-types for normal excitability and function (Ogiwara et al., 2007; Yu et al., 2006), suggesting the contributions of $Na_V1.1$ to neuronal function are highly sensitive to genetic perturbations. At the behavioral level, Scn1a-Het mice had an identical phenotype to Scn1a-cKO mice, moving more slowly and less than controls, despite not having the more severe and visible motor coordination deficits. Indeed, their performance on the rotarod was identical to that of Scn1a-floxed controls (**Fig 5**). How these behavioral differences arise given the similar transmission deficits in Scn1a-cKO and Scn1a-Het afferents is unclear. One possibility is a presynaptic role for $Na_V1.1$ in proprioceptive terminals that is unveiled when both copies of $Na_V1.1$ are lost. For example, loss of presynaptic $Na_V1.7$ channels in the spinal cord reduced glutamate release from nociceptive afferents onto dorsal horn neurons (MacDonald et al., 2021). If a similar mechanism is at play for $Na_V1.1$ in proprioceptors, reduced neurotransmitter release from Scn1a-Het afferent terminals could be sufficient to produce quantifiable, albeit more subtle, motor deficits. Future studies are required to test this possibility.

Notably, *Scn1a* is a super culprit gene with over one thousand associated disease-causing mutations, most of which are linked to different forms of epilepsy. Many epilepsy patients with

hemizygous $Na_V1.1$ loss-of-function display ataxia and motor delays and deficiencies (Claes et al., 2001; Fujiwara et al., 2003), which has traditionally been attributed to loss of $Na_V1.1$ function in the brain, namely the cerebellum (Kalume et al., 2007). Our findings suggest that some of the clinical manifestations associated with epilepsy are not solely due to $Na_V1.1$ loss-of-function in the brain, but also may manifest in part as a result from unreliable coding by peripheral proprioceptors.

Data presented in this study provide new evidence of a role for peripherally expressed $Na_V1.1$ in motor coordination. We show that $Na_V1.1$ is ubiquitously and strongly expressed in proprioceptors, contributes to proprioceptor excitability *in vitro* and *ex vivo,* and is haploinsufficient in sensory neurons for normal motor behaviors. Collectively, this works identifies a new role for $Na_V1.1$ in mammalian proprioception.

MATERIALS AND METHODS

Key resources. **Table 1** contains a list of key resources and supplies used for this study.

Key Resources Table

Reagent type or resource	Designation	Source or Reference	Identifiers	Additional information
Antibody	Rabbit polyclonal anti-DsRed	Takara Bio	Catalogue #632496	1:3000
Antibody	Chicken polyclonal GFP	Abcam	Catalogue #ab13970	1:3000
Antibody	Chicken polyclonal NFH	Abcam	Catalogue #ab4680	In muscle spindles: (1:300) In DRG: (1:3000)
Antibody	Rabbit polyclonal CGRP	Immunostar	Catalogue #24112	1:1000
Antibody	Guinea pig polyclonal VGLUT1	Zuckerman institute (Columbia University)	Catalogue #CU1706, RRID:AB_2665455	In spinal cord: (1:8000) In muscle spindles: (1:800)

Antibody	Chicken polyclonal β3-tubulin	Abcam	Catalogue #ab41489	1:500
Antibody	Rabbit polyclonal β3-tubulin	Abcam	Catalogue #ab18207	1:3000
Antibody	Rabbit polyclonal ChAT	Zuckerman institute (Columbia University)	Catalog #CU1574	1:10,000
Chemical compound, drug	VECTASHIELD® Antifade Mounting Media with DAPI	Vector Laboratories	Catalogue #H-2000	
Chemical compound, drug	Tissue-Tek OCT compound	Sakura	Catalogue #4583	
Chemical compound, drug	Laminin	Sigma-Aldrich	Catalogue #L2020-1MG	
Chemical compound, drug	Collagenase type P	Sigma-Aldrich	Catalogue #11213865001	
Chemical compound, drug	TrypLE Express	Thermofisher	Catalogue #12605-010	
Chemical compound, drug	MEM	Thermofisher	Catalogue #11095-080	
Chemical compound, drug	Penicillin-streptomycin	Thermofisher	Catalogue #15140-122	
Chemical compound, drug	MEM vitamin solution	Thermofisher	Catalogue #11120-052	
Chemical compound, drug	B-27 supplement	Thermofisher	Catalogue #17504-044	
Chemical compound, drug	Horse serum, heat inactivated	Thermofisher	Catalogue #26050-070	
Chemical compound, drug	ICA 121431	Tocris Bioscience	Catalogue #5066/10	
Chemical compound, drug	4,9 – anhydrous tetrodotoxin	Tocris Bioscience	Catalogue #6159	

Chemical compound, drug	PF- 05089771	Tocris Bioscience	Catalogue #5931	
Chemical compound, drug	Tetrodotoxin	Abcam	Catalogue ab120054	
Assay Kit	RNAscope Fluorescence Multiplex Kit	Advanced Cell Diagnostics	Catalogue #320851	
Oligonucleotide	*Pvalb* probe channel 1	Advanced Cell Diagnostics	Catalogue #421931	
Oligonucleotide	*Scn1a* probe channel 2	Advanced Cell Diagnostics	Catalogue #556181-C2	
Oligonucleotide	*Scn8a* probe channel 2	Advanced Cell Diagnostics	Catalogue #313341-C2	
Oligonucleotide	*Scn9a* probe channel 2	Advanced Cell Diagnostics	Catalogue #434191-C2	
Oligonucleotide	*Runx3* probe channel 3	Advanced Cell Diagnostics	Catalogue #451271-C3	
Mouse Strain	*Pirt*^{cre}	Dr. Xinzhong Dong		
Mouse Strain	*Rosa26*^{Ai14}	Jackson Laboratories	Stock #007914	
Mouse Strain	*Pvalb*^{cre}	Jackson Laboratories	Stock #008069	
Mouse Strain	Scn1a-floxed	UC Davis MMRRC	Stock # 041829-UCD	
Mouse Strain	*Mrgprd*^{GFP}	Zheng et al., 2019		
Software/ Algorithms	pClamp 11.2 Software Suite	Molecular Devices	https://www.moleculardevices.com	
Software/ Algorithms	Image J	Schneider et al. (2012)	https://imagej.nih.gov	
Software/ Algorithms	Prism 9	Graphpad	https://www.graphpad.com	
Software/ Algorithms	LabChart	ADInstruments	https://www.adinstruments.com/products/labchart	

Software/ Algorithms	MATLAB	MathWorks	https://www.mathworks.com	
Software/ Algorithms	Software, algorithm, custom (MATLAB)	This study	https://github.com/docth eagrif/Current-Clamp-Matlab-Code_O-Neil-DA	Current clamp experiments were analyzed with a custom written Matlab Script that is available on Github

660

661 ***Animals***. *Pirt*^{cre} mice were a kind gift from Dr. Xinzhong Dong (Johns Hopkins University).
662 *Rosa26*^{Ai14} (stock #007914; (Madisen et al., 2010)) and *Pvalb*^{cre} (stock # 008069) were obtained
663 from Jackson Laboratories. Scn1a-floxed (stock # 041829-UCD) mice were purchased from the
664 UC Davis MMRRC. *Mrgprd* mice were originally published in Zheng et al., 2019. All mice used
665 were on a mixed C57BL/6 background (non-congenic) Genotyping was outsourced to Transnetyx.
666 Animal use was conducted according to guidelines from the National Institutes of Health's Guide
667 for the Care and Use of Laboratory Animals and was approved by the Institutional Animal Care
668 and Use Committee of Rutgers University-Newark (PROTO201900161), UC Davis (#21947 and
669 #22438) and San José State University (#990, ex vivo muscle recordings). Mice were maintained
670 on a 12 h light/dark cycle, and food and water was provided *ad libitum*.

671

672 **Rotarod.** To assess motor coordination, a rotarod machine (IITC Life Sciences, Woodland Hills,
673 CA) that has an accelerating rotating cylinder was used. 8-10 week old mice of both sexes were
674 acclimated to the behavior room for 2 h prior to testing. Mice were assayed on the rotarod for 3
675 consecutive days, with 3 trials per day and an intertrial interval of at least 15 min. The average of
676 the three trials per day was used. The experimenter was blind to genotype.

677

678 **Open field test.** 8-10 week old mice of both sexes were acclimated to the behavior room for 2 h
679 prior to testing. The open field apparatus consisted of a black square sound attenuating box of

dimensions 40.6 cm × 40.6 cm. A camera suspended above the arena was connected to a computer running Ethovision XT software, which tracked animal movement and velocity. An animal was placed in the center of the arena and allowed to freely explore for a 10 min trial. The experimenter was blind to genotype.

Tissue processing. For spinal cord immunolabeling experiments, whole spinal columns from adult (8-15 weeks) *Pirt*^{Cre};*Rosa26*^{Ai14} and *Pirt*^{Cre};Scn1a-floxed animals of both sexes were harvested on ice. For Tdtomato IHC, spinal columns were fixed overnight at 4°C in 4% paraformaldehyde. For vesicular glutamate transporter 1 (VGLUT1) and choline acetyltransferase (ChAT) co-labeling experiments, spinal columns were fixed in 4% paraformaldehyde for 1 h on ice. Tissue was then placed in 30% sucrose solution overnight at 4°C. Following cryoprotection, tissue was embedded in optimal cutting temperature compound (OCT, Tissue-Tek® Sakura) and stored at -80ºC until sectioning. DRG from adult (8-15 weeks) animals of both sexes were harvested from thoracic spinal levels and fixed in 4% formaldehyde for 15 min at 4°C and were then incubated in 30% sucrose for 2-4 h at 4°C. DRG were embedded in OCT and stored at -80°C until sectioning.

Immunohistochemistry. Immunohistochemistry of spinal cord cryostat sections (30μm) was performed using the following primary antibodies: Rabbit anti-DsRed (1:3000, Takara Bio, 632496), guinea pig anti-VGLUT1 (1:8000, Zuckerman Institute, 1705), and rabbit anti-ChAT (1:10,000, Zuckerman Institute, 1574). Secondary antibodies used were as follows: anti-rabbit 594 (1:1000, ThermoFisher, A32740), anti-guinea pig 488 (1:1000, ThermoFisher, A11073), and anti-chicken 647 (ThermoFisher, A32733). Specimens were mounted with Fluoromount-G with DAPI (SouthernBiotech, 0100-20). EDL muscles used in *ex vivo* muscle afferent recordings were placed in ice cold 4% paraformaldehyde for 1 h followed by ice cold methanol for 15 min. Muscles

were incubated in blocking solution (0.3% PBS-T and 1% BSA) followed by incubation in primary antibodies (guinea pig anti-VGLUT1 1:800 and chicken anti-NFH 1:300, ThermoFisher ab4680) for 3-6 days at 4ºC. After primary antibody treatment, tissue was washed in blocking solution and treated with secondary antibody (anti-guinea pig 488 1:50 and anti-chicken 594 1:300, Invitrogen, WA316328) for 2-3 days. Specimens were mounted with VECTASHIELD® with DAPI (H-2000, Vector Laboratories). All specimens were imaged in three dimensions on a on a Zeiss LSM880 Airyscan confocal microscope. Images were analyzed using ImageJ software.

Multiplex* in situ *hybridization. Fixed-frozen DRG tissue from 8-15 week old mice of both sexes was cut in 25μm sections and placed on electrostatically coated slides. Sections were processed for RNA *in situ* detection using a modified version of the manufacturer's protocol ((Griffith et al., 2019), Advanced Cell Diagnostics) and the following probes: *Pvalb* (421931- C1, mouse), *Runx3* (451271-C3, mouse), *Scn1a* (556181-C2, mouse), *Scn8a* (313341-C2, mouse), and *Scn9a* (434191-C2, mouse). Following *in situ* hybridization, sections were incubated in blocking solution (5% normal goat serum, 0.1% PBS-T) for 1 h at RT. Tissue was then incubated in primary antibodies overnight at 4°C. The following antibodies were used: rabbit DsRed (1:3000, Takara Bio, 632496), rabbit β3-tubulin (1:3000, Abcam, ab18207), chicken β3-tubulin (1:500, Abcam, ab41489), rabbit CGRP (1:1000, Immunostar, 24112), chicken GFP (1:3000, Abcam, ab13970), and chicken NFH (1:3000, Abcam, ab4680). Tissue was treated with the following secondary antibodies for 45 min at RT: anti-rabbit 448 (1:1000, Invitrogen, A32731), 594 (1:1000, Invitrogen, A11037) and 647 (1:1000, Invitrogen, A32733), anti-chicken 488 (1:1000, Invitrogen, A32931) and 594 (1:1000, Invitrogen, A32740). Sections were washed and mounted with Fluoromount-G with DAPI and imaged in three dimensions (2μm axial steps) on an Olympus confocal (LV3000) using a 40X 0.90 NA water objective lens. Images were auto-thresholded and the probe signal integrated density for individual neurons was analyzed using ImageJ software. The coefficients

of variation for *Scn1a*, *Scn8a*, and *Scn9a* integrated densities were calculated in Prism 9.0 (GraphPad Software) using the following formula: CV = μ/σ *100.

DRG culture preparation. DRG were harvested from thoracic spinal levels of adult *Pvalb*^{cre};*Rosa*26^{Ai14} and *Pirt*^{cre};Scn1a-floxed (6-16 weeks) mice of both sexes and transferred to Ca^{2+}-free and Mg^{2+}-free HBSS solution (Invitrogen, 14170-112). Upon isolation, processes were trimmed, and ganglia were transferred into collagenase (1.5 mg/mL; Type P, Sigma-Aldrich, 11213865001) in HBSS for 20 min at 37°C followed by TrypLE Express (ThermoFisher, 12605-010) for 3 min with gentle rotation. TrypLE was neutralized with 10% horse serum (heat-inactivated; Invitrogen, 26050-070) and supplemented with culture media (MEM with L-glutamine, Phenol Red, without sodium pyruvate, ThermoFisher, 11095-080), containing 10,000 U/mL Penicillin-streptomycin (ThermoFisher, 15140-122), MEM Vitamin Solution (Invitrogen, 11120-052), and B-27 supplement (ThermoFisher, 17504-044). Serum containing media was decanted and cells were triturated using a fire-polished Pasteur pipette in the MEM culture media described above. Cells were resuspended and triturated using a plastic pipette tip. Cells were plated on glass coverslips that had been washed in 2M NaOH for at least 4 h, rinsed with 70% ethanol, UV-sterilized, and treated with laminin (0.05 mg/mL, Sigma-Aldrich, L2020-1MG) for 1 hour prior to plating. Cells were then incubated at 37°C in 5% CO_2. Cells were used for electrophysiology experiments 14-36 h post-plating.

In Vitro *Electrophysiology.* Whole-cell voltage-clamp recordings were made from dissociated DRG neurons using patch pipettes pulled from Model P-1000 (Sutter Instruments). Patch pipettes had a resistance of 3-5MΩ when filled with an internal solution containing the following (in mM): 140 CsF, 10 NaCl, 1.1 EGTA, .1 $CaCl_2$, 10 HEPES, and 2.5 MgATP, pH with CsOH to 7.2. Seals and whole-cell configuration were obtained in an external solution containing the following (in

mM): 145 NaCl, 5 KCl, 10 HEPES, 10 Glucose, 2 $CaCl_2$, 2 $MgCl_2$, pH 7.3 with NaOH, osmolarity ~320mOsm. Series resistance ranged from 6-11MΩ and was compensated by 70-80%. To isolate whole-cell sodium currents during voltage clamp experiments, a modified external solution was applied containing the following (in mM): 15 NaCl, 130 TEA-Cl, 10 HEPES, 2 $BaCl_2$, 13 glucose, 0.03 $CdCl_2$, pH 7.3 with NaOH, Osmolarity ~320mOsm. Voltage clamp recordings were performed at room temperature and current clamp recordings were conducted at 37ºC. Bath temperature was controlled and monitored using CL-100 (Warner Instruments).

Ex vivo *electrophysiology*. The effect of the loss of $Na_V1.1$ on muscle spindle afferent firing rates during muscle stretch and sinusoidal vibration was determined using an isolated muscle nerve preparation. The extensor digitorum longus muscle and innervating peroneal branch of the sciatic nerve were dissected from adult (2-4 month old) mice of both sexes. Muscles were held at optimal length (Lo), or the length of the muscle that maximal force of twitch contraction occurred. A series of nine 4 s ramp-and-hold stretches were given to 3 different stretch lengths repeated 3 times each (2.5%, 5%, and 7.5% Lo; ramp speed 40% Lo/s). A series of twelve 9 s sinusoidal vibrations were given (25, 50, and 100 μm amplitude; 10, 25, 50, and 100 Hz frequency). A one-minute rest was given between each length change. Firing rates during a 10 s baseline before stretch (resting discharge or RD) and the maximal firing rate during the ramp up phase of stretch (dynamic peak or DP) were calculated for all animals. We determined whether the response to static stretch was maintained consistently throughout the 4s stretch, as well as the coefficient of variability of the interspike interval (ISI) during the plateau phase of stretch (CV = Std Dev/Mean of ISI over the time period of 1.5-3.5s after end of ramp up). Average firing rate during the 9 s of vibration and whether the unit could entrain in a 1:1 fashion to vibration was also determined. Detailed methods can be found in Wilkinson et al., 2012.

780 ***Pharmacology.*** ICA 121431 (#5066), 4,9-Anhydrotetrodotoxin (AH-TTX, #6159), and PF-
781 05089771 (#5931) was purchased from Tocris Bioscience. Tetrodotoxin (TTX, ab120054) was
782 purchased from abcam. All other chemicals were from Sigma-Aldrich and Fisher Chemical.
783
784 ***Data acquisition and analysis***. Currents and voltages were acquired using pClamp software
785 v11.2 (Molecular Devices). Recordings were obtained using an AxoPatch 200b patch-clamp
786 amplifier and a Digidata 1550B and filtered at 5 kHz and digitized at 10 kHz. For biophysical
787 analysis of whole-cell sodium currents, conductance (G) was calculated as $G = I / (V - E_{Na})$, in
788 which *I* is the peak current, *V* is the voltage step, and E_{Na} is the reversal potential for sodium
789 calculated from Nernst equation based on the intracellular and extracellular sodium
790 concentrations in our recording solutions (10.38mV). Conductance data were normalized by the
791 maximum conductance value, G_{max}, and data was fit with the Boltzmann equation: Fraction
792 available = Minimum + ([Maximum-Minimum]/[1+exp(V50 Vm)/*k*]), where V_{50} denotes the
793 membrane potential at which half the channels are inactivated and *k* denotes the Boltzmann
794 constant/slope factor. For voltage dependence of steady state inactivation, peak current data
795 were normalized based on the maximum current, I_{max}. Analysis of action potential amplitude, full-
796 width half max, and threshold were performed on the first action potential elicited in response to
797 a 100 pA current injection (100 ms). Action potential threshold was calculated as the membrane
798 potential at which the first derivative of the somatic membrane potential (dV/dT) reached 10 mV
799 ms^{-1} (Griffith et al., 2019; Kress et al., 2008). Tau values were calculated from 20 ms voltage
800 steps from -90 mV to -30 mV and analyzed with single exponential curve fits. Voltage-clamp and
801 current-clamp experiments were analyzed with Clampfit software v11.2 (Molecular Devices) and
802 custom MatLab Scripts. *Ex vivo* recordings were obtained using an A-M Systems Model 1800
803 extracellular amplifier with headstage and digitized using an ADInstruments PowerLab. Data was
804 analyzed using ADInstruments LabChart software using the Spike Histogram function.
805

806 ***Experimental design and statistical analysis***. Summary data are presented as mean ± SEM,
807 from *n* cells or afferents, or *N* animals. For quantitative analysis of *in situ* hybridization data, at
808 least 3 biological replicates per condition were used and the investigator was blinded to genotype
809 for analysis. Behavioral experiments and analysis were also performed genotype-blind. Statistical
810 differences were determine using parametric tests for normally distributed data and non-
811 parametric tests for data that did not conform to Gaussian distributions or had different variances.
812 Statistical tests are listed in *Results* and/or figure legends. Statistical significance in each case is
813 denoted as follows: *p <0.05, **p < 0.01, ***p < 0.001, and ****p < 0.0001. Statistical tests and
814 curve fits were performed using Prism 9.0 (GraphPad Software). All data generated or analyzed
815 during this study are included in the manuscript and supporting file; Source Data files have been
816 uploaded to Mendeley for all figures. Code has been uploaded to GitHub. A key resources table
817 with specific organism and reagent information has been included in the method section.
818

REFERENCES

Ahern CA, Payandeh J, Bosmans F, Chanda B. 2016. The hitchhiker's guide to the voltage-gated sodium channel galaxy. *J Gen Physiol* **147**:1–24. doi:10.1085/jgp.201511492

Barbosa C, Tan Z-Y, Wang R, Xie W, Strong JA, Patel RR, Vasko MR, Zhang J-M, Cummins TR. 2015. Navβ4 regulates fast resurgent sodium currents and excitability in sensory neurons. *Mol Pain* **11**:60. doi:10.1186/s12990-015-0063-9

Bean BP. 2007. The action potential in mammalian central neurons. *Nat Rev Neurosci* **8**:451–465. doi:10.1038/nrn2148

Bennett DL, Clark AJ, Huang J, Waxman SG, Dib-Hajj SD. 2019. The Role of Voltage-Gated Sodium Channels in Pain Signaling. *Physiol Rev* **99**:1079–1151. doi:10.1152/physrev.00052.2017

Bewick GS, Banks RW. 2015. Mechanotransduction in the muscle spindle. *Pflugers Arch* **467**:175–190. doi:10.1007/s00424-014-1536-9

Bewick GS, Reid B, Richardson C, Banks RW. 2005. Autogenic modulation of mechanoreceptor excitability by glutamate release from synaptic-like vesicles: evidence from the rat muscle spindle primary sensory ending. *J Physiol* **562**:381–394. doi:10.1113/jphysiol.2004.074799

Carrasco DI, Vincent JA, Cope TC. 2017. Distribution of TTX-sensitive voltage-gated sodium channels in primary sensory endings of mammalian muscle spindles. *J Neurophysiol* **117**:1690–1701. doi:10.1152/jn.00889.2016

Catterall WA. 2017. Forty Years of Sodium Channels: Structure, Function, Pharmacology, and Epilepsy. *Neurochem Res* **42**:2495–2504. doi:10.1007/s11064-017-2314-9

Claes L, Del-Favero J, Ceulemans B, Lagae L, Van Broeckhoven C, De Jonghe P. 2001. De novo mutations in the sodium-channel gene SCN1A cause severe myoclonic epilepsy of infancy. *Am J Hum Genet* **68**:1327–1332. doi:10.1086/320609

de Nooij JC, Doobar S, Jessell TM. 2013. Etv1 inactivation reveals proprioceptor subclasses that reflect the level of NT3 expression in muscle targets. *Neuron* **77**:1055–1068. doi:10.1016/j.neuron.2013.01.015

Denomme N, Lukowski AL, Hull JM, Jameson MB, Bouza AA, Narayan ARH, Isom LL. 2020. The voltage-gated sodium channel inhibitor, 4,9-anhydrotetrodotoxin, blocks human Nav1.1 in addition to Nav1.6. *Neurosci Lett* **724**:134853. doi:10.1016/j.neulet.2020.134853

Ding J, Li X, Tian H, Wang L, Guo B, Wang Y, Li W, Wang F, Sun T. 2021. SCN1A Mutation-Beyond Dravet Syndrome: A Systematic Review and Narrative Synthesis. *Front Neurol* **12**:743726. doi:10.3389/fneur.2021.743726

Escayg A, Goldin AL. 2010. Sodium channel SCN1A and epilepsy: mutations and mechanisms. *Epilepsia* **51**:1650–1658. doi:10.1111/j.1528-1167.2010.02640.x

Florez-Paz D, Bali KK, Kuner R, Gomis A. 2016. A critical role for Piezo2 channels in the mechanotransduction of mouse proprioceptive neurons. *Sci Rep* **6**:25923. doi:10.1038/srep25923

Fujiwara T, Sugawara T, Mazaki-Miyazaki E, Takahashi Y, Fukushima K, Watanabe M, Hara K, Morikawa T, Yagi K, Yamakawa K, Inoue Y. 2003. Mutations of sodium channel alpha subunit type 1 (SCN1A) in intractable childhood epilepsies with frequent generalized tonic-clonic seizures. *Brain J Neurol* **126**:531–546. doi:10.1093/brain/awg053

862 Fukuoka T, Kobayashi K, Yamanaka H, Obata K, Dai Y, Noguchi K. 2008. Comparative study of
863 the distribution of the alpha-subunits of voltage-gated sodium channels in normal and
864 axotomized rat dorsal root ganglion neurons. *J Comp Neurol* **510**:188–206.
865 doi:10.1002/cne.21786

866 Griffith TN, Docter TA, Lumpkin EA. 2019. Tetrodotoxin-Sensitive Sodium Channels Mediate
867 Action Potential Firing and Excitability in Menthol-Sensitive Vglut3-Lineage Sensory Neurons. *J*
868 *Neurosci* **39**:7086–7101. doi:10.1523/JNEUROSCI.2817-18.2019

869 Herzog RI, Cummins TR, Ghassemi F, Dib-Hajj SD, Waxman SG. 2003. Distinct repriming and
870 closed-state inactivation kinetics of Nav1.6 and Nav1.7 sodium channels in mouse spinal
871 sensory neurons. *J Physiol* **551**:741–750. doi:10.1113/jphysiol.2003.047357

872 Ho C, O'Leary ME. 2011. Single-cell analysis of sodium channel expression in dorsal root
873 ganglion neurons. *Mol Cell Neurosci* **46**:159–166. doi:10.1016/j.mcn.2010.08.017

874 Kalume F, Yu FH, Westenbroek RE, Scheuer T, Catterall WA. 2007. Reduced sodium current in
875 Purkinje neurons from Nav1.1 mutant mice: implications for ataxia in severe myoclonic epilepsy
876 in infancy. *J Neurosci* **27**:11065–11074. doi:10.1523/JNEUROSCI.2162-07.2007

877 Khaliq ZM, Gouwens NW, Raman IM. 2003. The contribution of resurgent sodium current to
878 high-frequency firing in Purkinje neurons: an experimental and modeling study. *J Neurosci*
879 **23**:4899–4912.

880 Kress GJ, Dowling MJ, Meeks JP, Mennerick S. 2008. High Threshold, Proximal Initiation, and
881 Slow Conduction Velocity of Action Potentials in Dentate Granule Neuron Mossy Fibers. *J*
882 *Neurophysiol* **100**:281–291. doi:10.1152/jn.90295.2008

883 Kupari J, Usoskin D, Parisien M, Lou D, Hu Y, Fatt M, Lönnerberg P, Spångberg M, Eriksson B,
884 Barkas N, Kharchenko PV, Loré K, Khoury S, Diatchenko L, Ernfors P. 2021. Single cell
885 transcriptomics of primate sensory neurons identifies cell types associated with chronic pain.
886 *Nat Commun* **12**:1510. doi:10.1038/s41467-021-21725-z

887 Lin S-H, Cheng Y-R, Banks RW, Min M-Y, Bewick GS, Chen C-C. 2016. Evidence for the
888 involvement of ASIC3 in sensory mechanotransduction in proprioceptors. *Nat Commun*
889 **7**:11460. doi:10.1038/ncomms11460

890 Lossin C. 2009. A catalog of SCN1A variants. *Brain Dev* **31**:114–130.
891 doi:10.1016/j.braindev.2008.07.011

892 MacDonald DI, Sikandar S, Weiss J, Pyrski M, Luiz AP, Millet Q, Emery EC, Mancini F, Iannetti
893 GD, Alles SRA, Arcangeletti M, Zhao J, Cox JJ, Brownstone RM, Zufall F, Wood JN. 2021. A
894 central mechanism of analgesia in mice and humans lacking the sodium channel NaV1.7.
895 *Neuron* **109**:1497-1512.e6. doi:10.1016/j.neuron.2021.03.012

896 Madisen L, Zwingman TA, Sunkin SM, Oh SW, Zariwala HA, Gu H, Ng LL, Palmiter RD,
897 Hawrylycz MJ, Jones AR, Lein ES, Zeng H. 2010. A robust and high-throughput Cre reporting
898 and characterization system for the whole mouse brain. *Nat Neurosci* **13**:133–140.
899 doi:10.1038/nn.2467

900 Mendelsohn AI, Simon CM, Abbott LF, Mentis GZ, Jessell TM. 2015. Activity Regulates the
901 Incidence of Heteronymous Sensory-Motor Connections. *Neuron* **87**:111–123.
902 doi:10.1016/j.neuron.2015.05.045

903 Mulley JC, Scheffer IE, Petrou S, Dibbens LM, Berkovic SF, Harkin LA. 2005. SCN1A mutations
904 and epilepsy. *Hum Mutat* **25**:535–542. doi:10.1002/humu.20178

905 Nguyen MQ, von Buchholtz LJ, Reker AN, Ryba NJ, Davidson S. 2021. Single-nucleus
906 transcriptomic analysis of human dorsal root ganglion neurons. *eLife* **10**:e71752.
907 doi:10.7554/eLife.71752

908 Ogiwara I, Miyamoto H, Morita N, Atapour N, Mazaki E, Inoue I, Takeuchi T, Itohara S,
909 Yanagawa Y, Obata K, Furuichi T, Hensch TK, Yamakawa K. 2007. Nav1.1 localizes to axons
910 of parvalbumin-positive inhibitory interneurons: a circuit basis for epileptic seizures in mice
911 carrying an Scn1a gene mutation. *J Neurosci* **27**:5903–5914. doi:10.1523/JNEUROSCI.5270-
912 06.2007

913 Oliver KM, Florez-Paz DM, Badea TC, Mentis GZ, Menon V, de Nooij JC. 2021a. Molecular
914 correlates of muscle spindle and Golgi tendon organ afferents. *Nat Commun* **12**:1451.
915 doi:10.1038/s41467-021-21880-3

916 Oliver KM, Florez-Paz DM, Badea TC, Mentis GZ, Menon V, de Nooij JC. 2021b. Molecular
917 correlates of muscle spindle and Golgi tendon organ afferents. *Nat Commun* **12**:1451.
918 doi:10.1038/s41467-021-21880-3

919 Osteen JD, Herzig V, Gilchrist J, Emrick JJ, Zhang C, Wang X, Castro J, Garcia-Caraballo S,
920 Grundy L, Rychkov GY, Weyer AD, Dekan Z, Undheim EAB, Alewood P, Stucky CL, Brierley
921 SM, Basbaum AI, Bosmans F, King GF, Julius D. 2016. Selective spider toxins reveal a role for
922 the Nav1.1 channel in mechanical pain. *Nature* **534**:494–499. doi:10.1038/nature17976

923 Patel RR, Barbosa C, Xiao Y, Cummins TR. 2015. Human Nav1.6 Channels Generate Larger
924 Resurgent Currents than Human Nav1.1 Channels, but the Navβ4 Peptide Does Not Protect
925 Either Isoform from Use-Dependent Reduction. *PloS One* **10**:e0133485.
926 doi:10.1371/journal.pone.0133485

927 Pineda-Farias JB, Loeza-Alcocer E, Nagarajan V, Gold MS, Sekula RF. 2021. Mechanisms
928 Underlying the Selective Therapeutic Efficacy of Carbamazepine for Attenuation of Trigeminal
929 Nerve Injury Pain. *J Neurosci* **41**:8991–9007. doi:10.1523/JNEUROSCI.0547-21.2021

930 Salvatierra J, Castro J, Erickson A, Li Q, Braz J, Gilchrist J, Grundy L, Rychkov GY, Deiteren A,
931 Rais R, King GF, Slusher BS, Basbaum A, Pasricha PJ, Brierley SM, Bosmans F. 2018. NaV1.1
932 inhibition can reduce visceral hypersensitivity. *JCI Insight* **3**:121000.
933 doi:10.1172/jci.insight.121000

934 Sharma N, Flaherty K, Lezgiyeva K, Wagner DE, Klein AM, Ginty DD. 2020. The emergence of
935 transcriptional identity in somatosensory neurons. *Nature* **577**:392–398. doi:10.1038/s41586-
936 019-1900-1

937 Than K, Kim E, Navarro C, Chu S, Klier N, Occiano A, Ortiz S, Salazar A, Valdespino SR,
938 Villegas NK, Wilkinson KA. 2021. Vesicle-released glutamate is necessary to maintain muscle
939 spindle afferent excitability but not dynamic sensitivity in adult mice. *J Physiol* **599**:2953–2967.
940 doi:10.1113/JP281182

941 Usoskin D, Furlan A, Islam S, Abdo H, Lönnerberg P, Lou D, Hjerling-Leffler J, Haeggström J,
942 Kharchenko O, Kharchenko PV, Linnarsson S, Ernfors P. 2015. Unbiased classification of
943 sensory neuron types by large-scale single-cell RNA sequencing. *Nat Neurosci* **18**:145–153.
944 doi:10.1038/nn.3881

945 Wang W, Atianjoh F, Gauda EB, Yaster M, Li Y, Tao Y-X. 2011. Increased expression of
946 sodium channel subunit Nav1.1 in the injured dorsal root ganglion after peripheral nerve injury.
947 *Anat Rec Hoboken NJ 2007* **294**:1406–1411. doi:10.1002/ar.21437

948 Wangzhou A, McIlvried LA, Paige C, Barragan-Iglesias P, Shiers S, Ahmad A, Guzman CA,
949 Dussor G, Ray PR, Gereau RW, Price TJ. 2020. Pharmacological target-focused transcriptomic
950 analysis of native vs cultured human and mouse dorsal root ganglia. *Pain* **161**:1497–1517.
951 doi:10.1097/j.pain.0000000000001866

952 Wilkinson KA, Kloefkorn HE, Hochman S. 2012. Characterization of muscle spindle afferents in
953 the adult mouse using an in vitro muscle-nerve preparation. *PloS One* **7**:e39140.
954 doi:10.1371/journal.pone.0039140

955 Woo S-H, Lukacs V, de Nooij JC, Zaytseva D, Criddle CR, Francisco A, Jessell TM, Wilkinson
956 KA, Patapoutian A. 2015. Piezo2 is the principal mechanotransduction channel for
957 proprioception. *Nat Neurosci* **18**:1756–1762. doi:10.1038/nn.4162

958 Wu H, Petitpré C, Fontanet P, Sharma A, Bellardita C, Quadros RM, Jannig PR, Wang Y,
959 Heimel JA, Cheung KKY, Wanderoy S, Xuan Y, Meletis K, Ruas J, Gurumurthy CB, Kiehn O,
960 Hadjab S, Lallemend F. 2021. Distinct subtypes of proprioceptive dorsal root ganglion neurons
961 regulate adaptive proprioception in mice. *Nat Commun* **12**:1026. doi:10.1038/s41467-021-
962 21173-9

963 Yu FH, Mantegazza M, Westenbroek RE, Robbins CA, Kalume F, Burton KA, Spain WJ,
964 McKnight GS, Scheuer T, Catterall WA. 2006. Reduced sodium current in GABAergic
965 interneurons in a mouse model of severe myoclonic epilepsy in infancy. *Nat Neurosci* **9**:1142–
966 1149. doi:10.1038/nn1754

967 Zheng Y, Liu P, Bai L, Trimmer JS, Bean BP, Ginty DD. 2019a. Deep Sequencing of
968 Somatosensory Neurons Reveals Molecular Determinants of Intrinsic Physiological Properties.
969 *Neuron* **103**:598-616.e7. doi:10.1016/j.neuron.2019.05.039

970 Zheng Y, Liu P, Bai L, Trimmer JS, Bean BP, Ginty DD. 2019b. Deep Sequencing of

971 Somatosensory Neurons Reveals Molecular Determinants of Intrinsic Physiological Properties.

972 *Neuron* **103**:598-616.e7. doi:10.1016/j.neuron.2019.05.039

973